MAGNETORESISTANCE OF POTASSIUM

MAGNETORESISTANCE OF POTASSIUM

By

JOHANNA MARIA DAAMS, B.Sc.

A Thesis

Submitted to the School of Graduate Studies

in Partial Fulfilment of the Requirements

for the Degree

Master of Science

McMaster University

November 1974

MASTER OF SCIENCE (Physics)

McMASTER UNIVERSITY
Hamilton, Ontario

TITLE: Magnetoresistance of Potassium

AUTHOR: Johanna Maria Daams, B.Sc. (Queen's University)

SUPERVISOR: Professor J. P. Carbotte

NUMBER OF PAGES: (vi), 72

SCOPE AND CONTENTS:

The semi-classical path-integral method for finding the magnetoconductivity is specialised to cubic one-electron metals having a spherical Fermi surface, isotropic effective mass and anisotropic scatterimg times. Properties of the conductivity and resistivity tensors are deduced for this special case, in more detail for high magnetic fields. The magnetoconductivity for potassium, and the quantities derived from it - magnetoresistance and induced torque - are calculated as functions of temperature, field strength, impurity concentration and crystal orientation. Comparison is made with experimental results.

ACKNOWLEDGEMENTS

I would like to thank Dr. J. P. Carbotte, my research supervisor, for his guidance and encouragement.

I wish to thank Dr. R. J. Douglas for his assistance with the programming.

The financial assistance of the National Research Council is gratefully acknowledged.

I also wish to thank Miss Erie Long for her speedy and accurate typing of this thesis.

TABLE OF CONTENTS

LIST OF FIGURES

LIST OF FIGURES - continued

INTRODUCTION

In one-electron metals with spherical Fermi surfaces, the origin of the slight increase in the diagonal components of the resistivity tensor when a magnetic field is applied is the anisotropy of the scattering times. Until recently these scattering times could not be calculated for the alkalis with any degree of confidence, but now that this has been done, the problem of the magnetoresistance can be tackled using a semi-classical expression for the conductivity tensor that is known to work for aluminum. This thesis is concerned with the derivation of this expression, its symmetry properties and most important, its numerical value for potassium. Quantities derivable from the conductivity tensor - the resistivity tensor and induced torque - are also discussed and calculated numerically.

CHAPTER I

THEORY

A. The Boltzmann Equation

For a spatially homogeneous system which has reached a steady-state condition, the electric current density may be written

$$\underline{J} = - \sum_{\underline{k}} 2e\underline{v}(\underline{k}) f(\underline{k},T) \qquad (I.1)$$

where $2f(\underline{k})$ is the number of electrons per unit volume in the state $\underline{k}$, and $\underline{v}(\underline{k})$ the velocity of an electron at that point in reciprocal space. If we agree that $\underline{k}$, $f(\underline{k},T)$, and $\underline{v}(\underline{k})$ are well defined quantities, a reasonable assumption where the mean free path is much greater than the de Broglie wavelength, then the problem of finding the current set up by various external forces acting on the electrons is solved once $f(\underline{k},T)$ and $\underline{v}(\underline{k})$ are known.

This thesis is concerned more with $f(\underline{k},T)$ than $\underline{v}(\underline{k})$, which is assumed to be known. In fact, the simplest possible form for $\underline{v}(\underline{k})$ is assumed: $\underline{v}$ parallel to $\underline{k}$ with magnitude independent of direction. This is equivalent to a spherical Fermi surface with isotropic effective mass, which is a reasonable description of only a very few metals - in particular potassium, for which all the calculations were made.

The validity of these assumptions will be discussed in Section D.

Since we are interested in the combined effect of electric and magnetic fields on $\underline{J}$, $f(\underline{k},T)$ must satisfy the Boltzmann equation for a spatially homogeneous (no thermal gradients) system in magnetic and electric fields

$$-\frac{\partial f(\underline{k},T)}{\partial t} = +\frac{e}{\hbar}\left(\underline{E} + \frac{1}{c}\,\underline{v}(\underline{k}) \times \underline{H}\right)\cdot\nabla_{\underline{k}} f \quad . \tag{I.2}$$

This is basically a continuity equation in $\underline{k}$-space which assumes that $\hbar\dot{\underline{k}} = -e(\underline{E} + \frac{1}{c}\,\underline{v}(\underline{k}) \times \underline{H})$. Such an equation of motion for an electron moving in a crystal potential certainly requires justification, and is no trivial matter, but it is beyond the scope of this thesis. Finally, there is one more assumption to be made, namely that the L.S. of (I.2) can be approximated by $g(\underline{k},T)/\tau(\underline{k},T)$. (This substitution does not define $\tau(\underline{k},T)$.) $g(\underline{k},T)$ is the deviation from the equilibrium distribution $f_0(\underline{k},T)$

$$\begin{aligned} g(\underline{k},T) &= f(\underline{k},T) - f_0(\underline{k},T) \\ f_0(\underline{k},T) &= 1/(\exp\{(\varepsilon(\underline{k}) - \varepsilon_F)/k_B T\} + 1) \quad . \end{aligned} \tag{I.3}$$

Here $\varepsilon(\underline{k})$ is the energy of an electron in state $\underline{k}$, ε_F is the Fermi energy at temperature T, k_B is the Boltzmann constant,

and $\tau(\underline{k},T)$ is the anisotropic scattering time, which is assumed to be known throughout this thesis. Its origin is discussed in Section B. Substituting (I.3) into (I.2), dropping a term in $\underline{E}\cdot\nabla_{\underline{k}}g$ (a nonlinear term) and using $\nabla_{\underline{k}}f_0 = (\partial f_0/\partial\varepsilon)\hbar\underline{v}(\underline{k})$, we obtain the linearized Boltzmann equation

$$-\frac{\partial f_0}{\partial\varepsilon}\,\underline{v}(\underline{k})\cdot e\underline{E} = \frac{g(\underline{k},T)}{\tau(\underline{k},T)} + \frac{e}{\hbar c}\,(\underline{v}(\underline{k}) \times \underline{H})\cdot\nabla_{\underline{k}}g(\underline{k},T)\ . \qquad (I.4)$$

From now on the second argument, T, will be omitted except where temperature dependence is being discussed.

That nonlinear term was dropped to ensure that the solution $g(\underline{k})$ is linear in $\underline{E}$, because we will plug $g(\underline{k})$ into Eq. (I.1) to construct the conductivity tensor, which is a measure of the linear current response to an electric field

$$\underline{J} = -2\sum_{\underline{k}} e\underline{v}(\underline{k})\,(f_0(\underline{k}) + g(\underline{k}))$$

$$= -2\sum_{\underline{k}} e\underline{v}(\underline{k})\,g(\underline{k})\ .$$

The sum of $f_0\underline{v}$ cancels because an equilibrium distribution carries no current. The remaining sum can be rewritten in several ways as an integral

$$\underline{J} = -\frac{e}{4\pi^3}\int d^3\underline{k}\,\underline{v}(\underline{k})\,g(\underline{k}) \qquad (I.5)$$

$$\underline{J} = -\frac{e}{4\pi^3\hbar}\int d\varepsilon \int \frac{dS}{v_\perp(\varepsilon)}\,\underline{v}(\underline{k})\,g(\underline{k}) \quad . \qquad \text{(I.6)}$$

In (I.6), $\int dS$ indicates integration over a surface of constant energy, and $\hbar v_\perp(\varepsilon)$ is the component of $\nabla_{\underline{k}}\varepsilon$ normal to this surface. Since $g(\underline{k})$ is expected to be very like $\delta(\varepsilon-\varepsilon_F)$, (I.6) is the more useful form.

From Eq. (I.4) it is clear that g must be linear in the components of $\underline{E}$, therefore, (I.5) or (I.6) should yield the conductivity tensor σ_{ij} once $g(\underline{k})$ is known.

In a magnetic field, new quantum effects appear, which must be taken into consideration in determining the validity of the preceding semi-classical approach. When the spacing between Landau levels is of the same order as ε_F, problems occur. Because the electrons are no longer condensed inside a spherical constant-energy surface, the electron dynamics are altered, and $\tau(\underline{k})$ is also modified. It depends on the number of unoccupied allowed states near $\underline{k}$, a number which may change as forbidden regions open up between the Landau levels. Such phenomena occur when $\hbar\omega \sim \varepsilon_F$, i.e., the cyclotron frequency is $\sim 10^{15}$ sec^{-1}, corresponding to unobtainably high magnetic fields. When this spacing is smaller, of the order k_BT, effects such as the de Haas-Schubnikov oscillations in the electrical resistivity are observable, indicating that orbital quantization does play a role. The corresponding cyclotron frequency, for potassium at 4K is approximately 10^{11} radian-sec^{-1}. This determines the highest field for

which the semi-classical equation (I.2) is valid.

Cubic symmetry is assumed throughout this thesis since potassium crystallizes in the bcc structure at low temperatures. Some of the derived results are, however, true for non-cubic crystals.

B. The Scattering Times

When the matrix elements for scattering into and out of each state $|\underline{k}>$ due to interactions between the electron and the lattice are known, an expression for the transition rate $-(\partial f(\underline{k})/\partial t)$ into a state $|\underline{k}>$ can be found and the left side of Eq. (I.2) can be written explicitly. With this substitution, setting H = 0 and assuming the phonon distribution has not been changed by turning on the field (no phonon drag), (I.2) becomes an integro-differential equation

$$e\underline{E}\cdot\nabla_{\underline{k}} f_0(\underline{k}) = -\frac{\hbar}{k_B T}\sum_{\underline{k}'} (\phi(\underline{k}') - \phi(\underline{k}))f_0(\underline{k}) \times (1 - f_0(\underline{k}'))W_{\underline{k}}^{\underline{k}'} \qquad (I.7)$$

The $\phi(\underline{k})$ are defined by

$$g(\underline{k}) = \frac{1}{k_B T}\phi(\underline{k})f_0(\underline{k})(1 - f_0(\underline{k})) \qquad (I.8)$$

and $W_{\underline{k}}^{\underline{k}'}$, which depends only on the phonon spectrum and distribution, the electron-phonon interaction, and $f_0(\underline{k})$, is the probability of scattering occurring by this mechanism. It seems plausible that the deviation $\phi(\underline{k})$ should be as a first approximation proportional to the rate $e\underline{v}\cdot\underline{E}$ at which

an electron in $|\underline{k}>$ can absorb energy from the electric field

$$\phi(\underline{k}) = - e\tau_0(\underline{k},T)\underline{v}(\underline{k})\cdot\underline{E} \quad . \tag{I.9}$$

The scattering time $\tau_0(\underline{k},T)$ makes its appearance as an unknown parameter characterizing an approximate solution to the Boltzmann equation. When it is not independent of $\underline{k}$, it can no longer be interpreted as the relaxation time for the decay of the non-equilibrium distribution $f_0(\underline{k}) + g(\underline{k})$, although there is a close connection.

From (I.7) and (I.9) it is clear that $\tau_0(\underline{k},T)$ can be calculated when the $W_{\underline{k}}^{\underline{k}'}$ are known. This has been done numerically for the alkali metals by Hayman and Carbotte [8]. A function $\alpha^2_{TR}F$ was calculated that allows the $\tau_0(\underline{k},T)$ to be computed at 21 points on the irreducible 48^{th} of the F.S. for temperatures above 2K. They calculated $\tau_0(\underline{k},T)$ without phonon drag for several models of the scattering potential which gave different degrees of anisotropy for $\tau_0(\underline{k},T)$ and for its mean value. The $\tau_0(\underline{k},T)$ used throughout this thesis are those derived from the Ashcroft pseudopotential with $R_c = 1.0353$ Å, which was chosen because it gave the best agreement with the observed resistivity (50% deviation at worst) over a wide range of temperatures. All reasonable pseudopotentials produce $\tau_0(\underline{k},T)$ of the same shape at all temperatures - smooth functions with maxima in the {001}

directions falling off rapidly towards nearly constant values over the rest of the F.S. - but the height of these maxima above the surrounding plane is very sensitive to temperature and the choice of a pseudopotential. Around 4K, where the anisotropy is greatest, for the chosen pseudopotential $\tau_0(001) \sim 4\tau_0(111)$ (at this temperature there is agreement to within 30% between the observed resistivity and that calculated from our pseudopotential). This 4:1 ratio is believed to be an underestimate; there is evidence that $\tau_0(\underline{k},T)$ is actually more anisotropic. An upper bound is 10:1, the value derived from the Bardeen pseudopotential which is generally thought to overestimate the anisotropy (see Fig. 1).

In the preceding discussion, the sole scattering mechanism was assumed to be the electron-phonon interaction, whereas in real metals, there is also scattering by impurity atoms in the lattice. It is usually assumed in transport theory that their influence can be accounted for by defining a new scattering time $\tau(\underline{k},T)$

$$\frac{1}{\tau(\underline{k},T)} = \frac{1}{\tau_0(\underline{k},T)} + \frac{1}{\tau_{res}} \quad . \tag{I.10}$$

The form of (I.10) is justified by regarding $\tau_0(\underline{k},T)$ as a relaxation time. The quantity τ_{res} is a constant independent of temperature (unlike $\tau(\underline{k},T)$, which is a rapidly

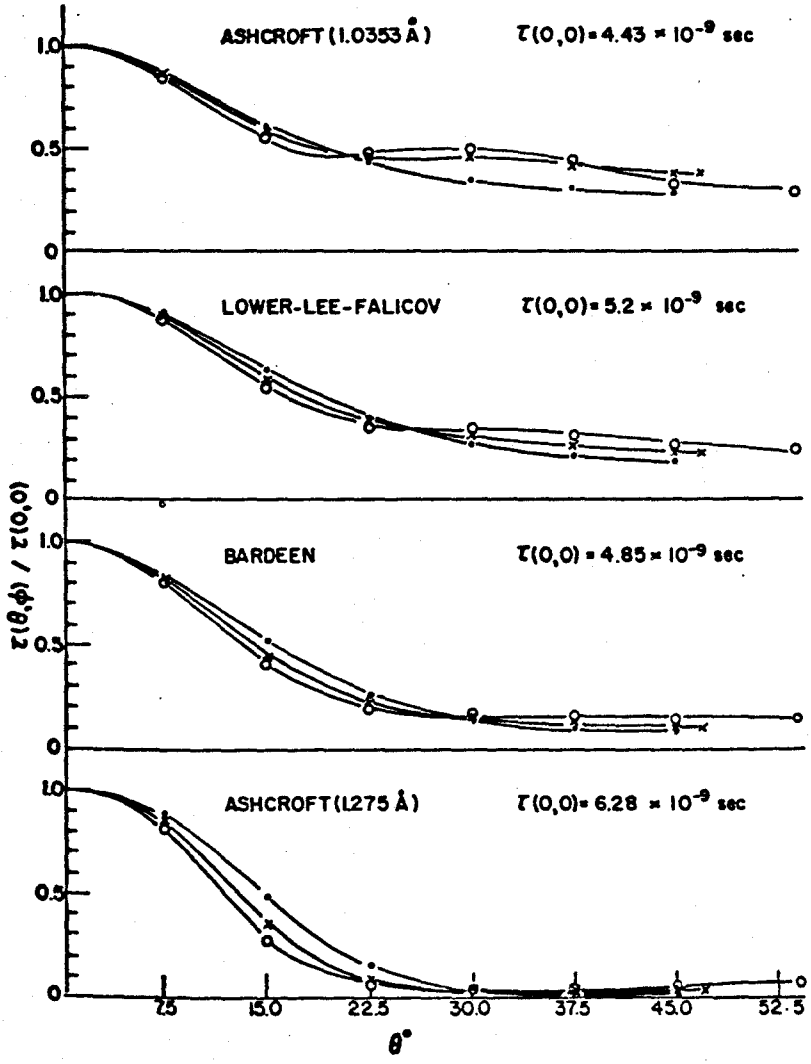

Scattering times in K at 4°K as a function of position on the irreducible $\frac{1}{48}$th of the Fermi surface. Results for various possible choices of pseudopotentials are compared. On each graph the value of $\tau(\bar{k})$ for $\bar{k} = (0, 0, k_F)$ is entered and all results are normalized to this value. For $\bar{k} \equiv (\theta, \phi, k_F)$, the results for the three arcs $\phi = 0°$, $22\frac{1}{2}°$, and $45°$ are to be distinguished as follows: •, $\phi = 0°$; ×, $\phi = 22\frac{1}{2}°$; o, $\phi = 45°$.

Fig. 1

As calculated by Hayman and Carbotte [24].

decreasing function of temperature) and will be assumed isotropic throughout this thesis, although recent calculations [25] show that it may vary by about 20% over the F.S. because of lattice strains. Therefore, $\tau(\underline{k},T)$ will be smaller and less anisotropic than $\tau_0(\underline{k},T)$, but the shape will be the same.

Still within the framework of the preceding approximations, and using cubic symmetry, the conductivity tensor may be written

$$\sigma_{ij}(T) = -\frac{e^2}{4\pi^3\hbar}\int_0^\infty d\varepsilon\,\frac{\partial f_0}{\partial\varepsilon}\int\frac{dS}{v_\perp(\varepsilon,\underline{k})}\,v_i(\underline{k})\,v_j(\underline{k})\,\tau(\underline{k},T)$$

$$\simeq \frac{Ne^2}{m^*}\,\langle\overline{\tau(\underline{k},T)}\rangle\delta_{ij} = \sigma_0\delta_{ij}\quad . \tag{I.11}$$

(The bar and brackets denote a Fermi surface average.) Cubic symmetry was used to get the second line.

The approximation involved in the second line is replacing $\int_0^\infty (\partial f_0/\partial\varepsilon)\,d\varepsilon$ by $\delta(\varepsilon-\varepsilon_F)$, strictly true only as $T \to 0$. This approximation is unavoidable in the course of these calculations, since $\tau(\underline{k},T)$ is not known off the F.S. Since we never deal with temperatures above 25K, it is perfectly justified. Because $\lim_{T\to 0}(1/\tau_0(\underline{k},T)) = 0$, the asymptotic value of σ_0, $Ne^2/m^*\,\tau_{res}$, allows τ_{res}, the residual scattering time, to be determined experimentally by extrapolating $\rho(T)$ to $T = 0$. The residual resistivity ρ_{res}

is defined as $(m^*/Ne^2)(1/\tau_{res})$. Note that

$$\rho_0(T) \equiv \frac{m^*}{Ne^2} \frac{1}{\langle \tau(\underline{k}) \rangle}$$

is only approximately equal to

$$\frac{m}{Ne^2} \left(\frac{1}{\langle \tau_0(\underline{k},T) \rangle} + \frac{1}{\tau_{res}} \right) \quad .$$

The subscript on ρ_0 indicates the absence of the magnetic field which is introduced in the next section, not the absence of impurities.

C. The Low-Field Limit: Method of Jones and Zener

According to this method [1], Eq. (I.2) is rewritten

$$(1+\Omega)g(\underline{k}) = -\tau(\underline{k})e\underline{E}\cdot\underline{v}(\underline{k})\frac{\partial f_0}{\partial \varepsilon} \qquad (I.12)$$

where $\Omega \equiv (e\tau(\underline{k})/\hbar c)(\underline{v}\times\underline{H})\cdot\nabla_{\underline{k}}$.

When H is small, it seems plausible that the operator $1+\Omega$ may be inverted, so that (I.12) becomes

$$g(\underline{k}) = (1 - \Omega + \Omega^2 - \Omega^3 \ldots)\{-\tau(\underline{k})e\underline{E}\cdot\underline{v}\frac{\partial f_0}{\partial \varepsilon}\} \quad . \qquad (I.13)$$

Since $\underline{J} = -2\sum_{\underline{k}} e\underline{v}g(\underline{k})$, Eq. (I.13) suggests that $\underline{J}$ may be written as a sum of powers of H

$$J_\alpha = \sigma^{(0)}_{\alpha\beta}E_\beta + \sigma^{(1)}_{\alpha\beta\gamma}E_\beta H_\gamma + \sigma^{(2)}_{\alpha\beta\gamma\delta}E_\beta H_\gamma H_\delta \ldots \qquad (I.14)$$

The expressions for these coefficients of expansion are complicated, especially when the coordinate axes are not aligned with the cube axes, and it is easier to introduce cubic symmetry immediately so that their number is reduced.

According to Seitz [2], when the Cartesian axes are aligned with the cube axes, the components of the current must have the form

$$J_\mu = \sigma_0 E_\mu + \alpha \varepsilon_{\mu\nu\lambda} E_\nu H_\lambda + \beta E_\mu H^2 + \gamma H_\mu (\underline{H}\cdot\underline{E})$$

$$+ \delta E_\mu H_\mu^2 + \text{terms of higher order} \qquad \text{(I.15)}$$

where $\varepsilon_{\mu\nu\lambda}$ is the Levi-Civita symbol, σ_0 is the zero-field conductivity and α, β, γ, and δ are constants depending only on $\underline{v}(\underline{k})$ and $\tau(\underline{k})$. Comparison of (I.14) and (I.15) shows that only $\sigma^{(0)}_{\alpha\beta}$, $\sigma^{(1)}_{\alpha\beta z} = \alpha\varepsilon_{\alpha\beta z}$ and the three $\sigma^{(2)}_{\alpha\alpha zz}$, are non-zero when H is along z and the cube axes lie along the coordinate axes. Even if H had not been along the z axis, only another 12 of the $\sigma^{(2)}_{\alpha\beta\gamma\delta}$ would have been non-vanishing, namely $\sigma^{(2)}_{\alpha\beta\beta\alpha} = \sigma^{(2)}_{\beta\alpha\alpha\beta} = \sigma^{(2)}_{\alpha\beta\alpha\beta} = \sigma^{(2)}_{\beta\alpha\beta\alpha}$. We will now write the coefficients α, β, γ, and δ in terms of the $\sigma^{(2)}_{\alpha\beta\gamma\delta}$, because only the former have well defined transformation properties and convenient analytic expressions [3] exist for the latter.

$$\sigma_0 = \sigma^{(0)}_{\alpha\beta}\delta_{\alpha\beta}$$

$$\alpha = \sigma^{(1)}_{xyz} = \frac{-e^3}{4\pi^3\hbar c}\int \frac{dS}{v_F}\{\tau^2 \frac{v_x^2}{m^*} - \tau v_x v_y (v_y \frac{\partial\tau}{\partial k_x} - v_x \frac{\partial\tau}{\partial k_y})\}$$

$$= -\frac{Ne^2}{m^*}\frac{\omega}{H}\overline{\langle\tau^2\rangle} \qquad \text{(I.16)}$$

$$\beta = \sigma^{(2)}_{xxzz} = \sigma^{(2)}_{yyzz} = -\varepsilon_{\rho z\nu}\varepsilon_{\mu z\sigma}\frac{e^4}{4\pi^3\hbar^2c^2}\int \frac{dS}{v_F}$$

$$\times \tau v_x v_\rho \frac{\partial}{\partial k_\nu}\{\tau v_\mu \frac{\partial}{\partial k_\sigma}(\tau v_x)\}$$

$$= -\frac{Ne^2}{m^*}\frac{\omega^2}{H^2}\tau^3 \quad \text{if } \tau \text{ is isotropic} \tag{I.17}$$

$$\beta + \gamma + \delta = \sigma^{(2)}_{zzzz} = -\varepsilon_{\rho z\nu}\varepsilon_{\mu z\sigma}\frac{e^4}{4\pi^3\hbar^2c^2}\int\frac{dS}{v_F} \times \tau v_z v_\rho \frac{\partial}{\partial k_\nu}\{\tau v_\mu \frac{\partial}{\partial k_\sigma}(\tau v_z)\}$$

$$= 0 \quad \text{if } \tau \text{ is isotropic .} \tag{I.18}$$

With a little more effort, we might have built up a few more equations like (I.17) and (I.18), thus enabling us to separate out γ and δ. This was not done because the values of the $\sigma^{(2)}_{\alpha\beta\gamma\delta}$ are not easily related qualitatively to the shape of $\tau(\underline{k})$.

According to convention the conductivity tensor is resolved on axes having z parallel to the magnetic field. Let the matrix $A_{\mu\nu}$ effecting the transformation from the cube axes to these new (primed) axes be such that $H'_\alpha = \delta_{\alpha z}H = A_{\alpha\mu}H_\mu$. Then, making use of the expression $J'_\alpha = A_{\alpha\mu}J_\mu$ and (I.15), we obtain

$$\sigma'_{xx} = \sigma_0 + \beta H^2 + (\sum_\mu A^2_{x\mu} A^2_{z\mu}) H^2\delta + \text{terms of higher even order in H}$$

$$\sigma'_{yy} = \sigma_0 + \beta H^2 + (\sum_\mu A^2_{y\mu} A^2_{z\mu}) H^2\delta + \text{terms of higher even order in H}$$

$$\sigma'_{zz} = \sigma_0 + (\beta+\gamma) H^2 + (\sum_\mu A^4_{z\mu}) H^2\delta + \text{terms of higher even order in H} \qquad \text{(I.19)}$$

$$\sigma'_{xy} = \alpha H + (\sum_\mu A_{x\mu} A_{y\mu} A_{z\mu}) H^2\delta + \text{higher order terms, odd or even}$$

$$\sigma'_{xz} = (\sum_\mu A_{x\mu} A^3_{z\mu}) H^2\delta + \text{higher order terms, odd or even}$$

$$\sigma'_{yz} = (\sum_\mu A_{y\mu} A^3_{z\mu}) H^2\delta + \text{higher order terms, odd or even} \ .$$

(Note that we could not have written $\sigma'_{\alpha\beta} = A_{\alpha\mu} A_{\beta\nu} \sigma_{\mu\nu}$ because $\sigma'_{\alpha\beta}$ is a tensor function of the orientation of $\underline{H}$ with respect to the crystal axes.)

Equations (I.19) show that the variations in $\sigma'_{\alpha\beta}$ as $\underline{H}$ changes direction can be predicted exactly from cubic symmetry alone, and that only the magnitude of these variations depends on $\tau(\underline{k})$ and its derivatives. This fact makes the low-field limit uninteresting, since only a very accurate knowledge of $\tau(\underline{k})$ permits a reasonable guess at the coefficient δ responsible for the anisotropy of $\tau(\underline{k})$ (because δ depends so much on the derivatives of $\tau(\underline{k})$). However, Eqs. (I.19) are still very useful for checking numerical calculations.

We now continue working in the new axes but drop the primes. The conductivity tensor (I.19) may be inverted to give. (N is the number of electrons per unit volume.)

$$\rho_{xx} = \frac{1}{\sigma_0} - \frac{H^2}{\sigma_0^2}\{(\beta + \delta \sum_{\mu} A_{x\mu}^2 A_{z\mu}^2) + \frac{\alpha^2}{\sigma_0}\} \ldots$$

$$\rho_{yy} = \frac{1}{\sigma_0} - \frac{H^2}{\sigma_0^2}\{(\beta + \delta \sum_{\mu} A_{y\mu}^2 A_{z\mu}^2) + \frac{\alpha^2}{\sigma_0}\} \ldots$$

$$\rho_{zz} = \frac{1}{\sigma_0} - \frac{H^2}{\sigma_0^2}\{\beta + \gamma + \delta \sum_{\mu} A_{z\mu}^4\} \ldots$$

$$\rho_{xy} = \frac{1}{Nec} \frac{\overline{<\tau^2>}}{\overline{<\tau>}^2} H - \frac{\delta H^2}{\sigma_0^2} \sum_{\mu} A_{x\mu} A_{y\mu} A_{z\mu} \ldots \qquad \text{(I.20)}$$

$$\rho_{xz} = -\frac{H^2\delta}{\sigma_0^2} \sum_{\mu} A_{x\mu} A_{z\mu}^3 + \frac{H^3\alpha\delta}{\sigma_0^3} \sum_{\mu} A_{y\mu} A_{z\mu}^3 \ldots$$

$$\rho_{yz} = -\frac{H^2\delta}{\sigma_0^2} \sum_{\mu} A_{y\mu} A_{z\mu}^3 - \frac{H^3\alpha\delta}{\sigma_0^3} \sum_{\mu} A_{x\mu} A_{z\mu}^3 \ldots \quad .$$

The Onsager relation $\sigma_{\alpha\beta}(H) = \sigma_{\beta\alpha}(-H)$ also implies $\rho_{\alpha\beta}(H) = \rho_{\beta\alpha}(-H)$; from this the remaining components of ρ_{ij} can be deduced.

When $\tau(\underline{k})$ is isotropic, (I.19) simplifies to

$$\sigma_{xx} = \sigma_{yy} = \sigma_0(1 + (\omega\tau)^2)$$

$$\sigma_{zz} = \sigma_0 \qquad \text{(I.21)}$$

$$\sigma_{xy} = -\sigma_0(\omega\tau)$$

while all other components vanish. The effect of isotropy on $\rho_{\alpha\beta}$ is even more dramatic

$$\rho_{\alpha\beta} = \rho_0 \delta_{\alpha\beta} \quad , \text{ except}$$

$$\rho_{xy} = \frac{m^*\omega}{Ne^2} = \frac{H}{Nec} \quad . \tag{I.22}$$

The magnetic field has no effect on currents parallel to the electric field; without anisotropy there is no low-field increase in $\rho_{\alpha\alpha}$. We shall see that this is true for any field strength.

D. The Chambers Path Integral

In a magnetic field an electron will follow a circular path modified by scattering, external electric fields and the crystal potential (which only alters the relation between $\underline{v}$ and $\underline{k}$). Since circular orbits are, therefore, fundamental to transport properties in a magnetic field, it may be useful to express the linearized Boltzmann equation (I.4) in non-Cartesian coordinates with the vertical axis parallel to $\underline{H}$. The position of an electron in $\underline{k}$-space is then specified not by (k_x,k_y,k_z) but (k_z,ϕ,ε). ε is just the energy, together with k_z it specifies which orbit we are dealing with, provided the F.S. does not cross the boundaries of the first Brillouin zone, and ϕ is a new angular variable which measures the position of an electron within a given orbit. ϕ is formally defined as

$$\phi(k_x,k_y,k_z) = + \omega \frac{\hbar c}{eH} \oint_{(k_{x0},0,k_z)}^{(k_x,k_y,k_z)} \frac{dk_{||}}{v_\perp} \quad \text{(counter clockwise)} \tag{I.23}$$

ω is the cyclotron frequency and k_{x0} is the value of k_x when the orbit (specified by k_z and ε) crosses the k_x axis. A different "starting point" for the orbit, other than the k_x axis could have been chosen, but this is conventional. $dk_{||}$ is the increment in $\underline{k}$ parallel to the orbit. From the form of the equation it is clear that ϕ must lie between 0 and 2π,

and for a spherical F.S., ϕ is just the azimuthal angle. But when a given electron is followed as it makes several orbits, $|\phi|$ may increase beyond 2π. ϕ has a very simple time dependence

$$\dot{\phi} = -\omega$$

so that (I.4) becomes

$$+\frac{\partial f_0}{\partial \varepsilon}\,\underline{v}(\underline{k})\cdot e\underline{E} = \frac{g(\underline{k})}{\tau(\underline{k})} + \dot{\phi}\,\frac{\partial f}{\partial \phi}$$

$$= \frac{g(\underline{k})}{\tau(\underline{k})} - \omega\,\frac{\partial g}{\partial \phi} \qquad \text{(I.24)}$$

f_0 depends on $\underline{k}$ only through $\varepsilon(\underline{k})$, and an orbit remains on the same constant energy surface, therefore $\partial f_0/\partial\phi = 0$. A formal solution to (I.24) developed by Shockley [4] is

$$g(\phi) = +\int_{\phi}^{\infty} d\phi' e\,\frac{\partial f_0}{\partial \varepsilon}\,\frac{\underline{E}\cdot\underline{v}(\phi')}{\omega}\,\exp\{-\int_{\phi}^{\phi'} d\phi''/(\omega\tau(\phi''))\}\,. \qquad \text{(I.25)}$$

(The dependence of $\underline{v}$ on k_z and ε and of τ on k_z, ε, and T will be omitted in the rest of this section.) Note that on a spherical surface ω is constant over the F.S.. The differential equation (I.24) has another solution, corresponding to the homogeneous form of the equation (with $\underline{E} = 0$). Adding on such a solution to (I.25) would have no

effect on the current.

From (I.25) the α component of $\underline{J}$ may be found

$$J_\alpha = -2e \sum_{\underline{k}} v_\alpha g(\underline{k})$$

$$= -\frac{e}{4\pi^3} \int d^3\underline{k} v_\alpha g(\underline{k}) \quad .$$

In the new coordinates, $d^3k = \frac{m^*}{\hbar^2} dk_z d\varepsilon d\phi$, so that

$$J_\alpha = \frac{-em^*}{4\pi^3\hbar^2} \int_0^\infty d\varepsilon \int dk_z \int_0^{2\pi} d\phi g(\phi) v_\alpha(\phi) \quad . \qquad \text{(I.26)}$$

If E is directed along axis β, then substituting (I.25) in (I.26) leads to (the dependence on k_z is implicit)

$$J_\alpha = -\frac{e^2 m^*}{4\pi^3\hbar^2} \int_0^\infty \frac{\partial f_0}{\partial \varepsilon} d\varepsilon \int dk_z \int_0^{2\pi} d\phi v_\alpha(\phi) \int_\phi^\infty d\phi' v_\beta(\phi')$$

$$\times \exp\{-\int_\phi^{\phi'} \frac{d\phi''}{\omega\tau(\phi'')}\} E_\beta \quad . \qquad \text{(I.27)}$$

The quantity between E_β and the equal sign is $\sigma_{\alpha\beta}$. The periodicity of all the variables in ϕ permits one more simplification. Let $\phi' = \phi_0' + 2n\pi$, $(n \geq 0, \phi < \phi_0' < 2\pi + \phi)$. Then the integral over ϕ' may be written

$$\sum_{n=0}^{\infty} \exp\{-n \int_0^{2\pi} \frac{d\phi''}{\omega\tau(\phi'')}\} \int_\phi^{\phi+2\pi} d\phi_0' v_\beta(\phi_0')$$

$$\times \exp\{-\int_\phi^{\phi_0'} \frac{d\phi''}{\omega\tau(\phi'')}\} \quad . \qquad \text{(I.28)}$$

At this point we introduce some notation

$$\frac{1}{\hat{\tau}} \equiv \frac{1}{2\pi}\int_0^{2\pi} \frac{d\phi}{\tau(\phi)}$$

$$g \equiv \frac{1}{\omega\hat{\tau}} \quad \text{(not to be confused with the deviation function } f(\underline{k}) - f_0(\underline{k})\text{)} \tag{I.29}$$

$$\gamma(\phi) \equiv \frac{\hat{\tau}}{\tau(\phi)} \quad .$$

These three quantities are all functions of k_z and ε. In the new notation

$$\sigma_{\alpha\beta} = \frac{-e^2 m^*}{4\pi^3 \hbar^2 \omega}\int_0^{\infty} \frac{\partial f_0}{\partial \varepsilon}\, d\varepsilon \int dk_z \frac{1}{1 - e^{-2\pi g}} \int_0^{2\pi} d\phi v_\alpha(\phi)$$

$$\times \int_{\phi}^{\phi+2\pi} d\phi' v_\beta(\phi') \exp\{-g\int_{\phi}^{\phi'} \gamma(\phi'')d\phi''\} \quad . \tag{I.30}$$

In going from (I.28) to (I.30), the redundant subscript on ϕ_0' was dropped.

Expression (I.30) is the well-known Chambers path integral. It is valid for any magnetic field subject to the limitations discussed at the end of Section A. However, an expansion in powers of H^{-1} is possible only $g < 1$, hence the need for Section C. The following expansion was first given by Chambers [5].

(a) The High-Field Limit

$$\sigma_{\alpha\beta} = \frac{-e^2 m^*}{4\pi^3 \hbar^2} \int_0^\infty \frac{\partial f_0}{\partial \varepsilon} d\varepsilon \int dk_z \hat{\tau} [A_{\alpha\beta 0} + gA_{\alpha\beta 1} + g^2 A_{\alpha\beta 2} \ldots] . \tag{I.31}$$

The $A_{\alpha\beta n}$ are defined in terms of the Fourier coefficients of v_α, v_β, and γ about the orbits

$$v_\alpha(\phi) = \sum_m v_{\alpha m} e^{im\phi}$$

$$\gamma(\phi) = \sum_m \gamma_n e^{im\phi} .$$

Being the Fourier coefficients of real functions, the γ_n and v_n satisfy $\gamma_n = \gamma^*_{-n}$ and $v_n = v^*_{-n}$.

$$A_{\alpha\beta 0} = v_{\alpha 0} v_{\beta 0}$$

$$A_{\alpha\beta 1} = i \sum_{n\neq 0} n^{-1} [v^*_{\alpha n} v_{\beta n} + \gamma_n (v_{\alpha 0} v^*_{\beta n} - v_{\beta 0} v^*_{\alpha n})]$$

$$A_{\alpha\beta 2} = \sum_{n\neq 0} n^{-2} v^*_{\alpha n} v_{\beta n} + \sum_{\substack{n\neq 0 \\ m\neq 0}} m^{-1} n^{-1} \{\gamma_n [v_{\alpha m} v^*_{\beta (m+n)} + v_{\beta m} v^*_{\alpha (m+n)}] - \gamma_m \gamma_n [\tfrac{1}{2} v_{\alpha 0} v^*_{\beta (m+n)} + \tfrac{1}{2} v_{\beta 0} v_{\alpha (m+n)} - v^*_{\alpha m} v^*_{\beta n}]\} \tag{I.32}$$

cont'd.

$$A_{\alpha\beta 3} = - i \sum_{n\neq 0} n^{-3} v^*_{\alpha n} v_{\beta n} + i \sum_{\substack{m\neq 0 \\ n\neq 0}} m^{-2} n^{-1} \gamma_n$$

$$\times [v_{\alpha m} v^*_{\beta (m+n)} - v_{\beta m} v^*_{\alpha (m+n)}] + \ldots$$

$$A_{\alpha\beta 4} = - \sum_{n\neq 0} n^{-4} v^*_{\alpha n} v_{\beta n} - \sum_{\substack{m\neq 0 \\ n\neq 0}} m^{-3} n^{-1} \gamma_n$$

$$\times [v_{\alpha m} v^*_{\beta (m+n)} - v_{\beta m} v^*_{\alpha (m+n)}] + \ldots \qquad \text{(I.32)}$$

Some terms in $\gamma_m \gamma_n$ were omitted from $A_{\alpha\beta 3}$ and $A_{\alpha\beta 4}$. These coefficients are particularly simple for a spherical surface, since of the $v_{\alpha n}$ only v_{z0}, $v_{z\pm 1}$, and $v_{y\pm 1}$ are non-vanishing. The γ_n are of course not limited in this way. In the spherical case ($k_\perp = \sqrt{k_F^2 - k_z^2}$)

$$A_{\alpha\beta 0} = 0 \quad \text{unless } \alpha = \beta = z, \text{ then } A_{zz0} = \left(\frac{\hbar k_z}{m^*}\right)^2$$

$$A_{\alpha\alpha 1} = 0$$

$$A_{xy1} = - A_{yx1} = -\frac{1}{2}\left(\frac{\hbar k_\perp}{m^*}\right)^2 = -\frac{1}{2\pi}\left(\frac{\hbar}{m^*}\right)^2 \times \text{area of orbit in } \underline{k}\text{-space}$$

$$A_{xz1} = - A_{zx1} = \frac{i}{2}\left(\frac{\hbar k_F}{m^*}\right)^2 \cos\beta\sin\beta\,(\gamma_{-1} - \gamma_1)$$

$$A_{yz1} = - A_{zy1} = \frac{1}{2}\left(\frac{\hbar k_F}{m^*}\right)^2 \cos\beta\sin\beta\,(\gamma_1 + \gamma_{-1})$$

$$A_{xx2} = \left(\frac{\hbar k_\perp}{2m^*}\right)^2 [2 - (\gamma_{-2} + \gamma_2) + (\gamma_1 - \gamma_{-1})^2] \qquad \text{(I.33)}$$

cont'd.

$$A_{yy2} = (\frac{\hbar k_\perp}{2m^*})^2 [2 + (\gamma_{-2} + \gamma_2) - (\gamma_1 + \gamma_{-1})^2]$$

$$A_{zz2} = -\frac{1}{2} (\frac{\hbar k_z}{m^*})^2 \gamma_1\gamma_{-1}$$

$$A_{yx2} = A_{xy2} = + i(\frac{\hbar k_\perp}{2m^*})^2 (-\gamma_{-1}^2 + \gamma_1^2)$$

$$A_{xz2} = A_{zx2} = -\frac{1}{2} (\frac{\hbar k_F}{m^*})^2 \sin\beta\cos\beta(\gamma_1 + \gamma_{-1})$$

$$A_{yz2} = A_{zy2} = \frac{i}{2} (\frac{\hbar k_F}{m^*})^2 \sin\beta\cos\beta(-\gamma_{-1} + \gamma_1)$$

$$A_{xx3} = A_{yy3} = A_{zz3} = 0$$

$$A_{xy3} = 0 + \text{possibly terms in } \gamma_m\gamma_n$$

$$A_{xz3} = -A_{zx3} = \frac{i}{2} (\frac{\hbar k_F}{m^*})^2 \sin\beta\cos\beta(\gamma_{-1} - \gamma_1)$$

$$+ \text{possibly more terms}$$

$$A_{yz3} = -A_{zy3} = -\frac{1}{2} (\frac{\hbar k_F}{m^*})^2 \sin\beta\cos\beta(\gamma_1 + \gamma_{-1})$$

$$+ \text{possibly more terms}$$

$$A_{xx4} = A_{yy4} = -\frac{1}{2} (\frac{\hbar k_\perp}{m^*})^2 + \text{possibly more terms}$$

$$A_{zz4} = 0 + \text{possibly more terms} \quad . \qquad (I.33)$$

The angle β is just the angle $\underline{k}$ makes with the z-axis.

It can be seen that the $A_{\alpha\beta n}$ satisfy $A_{\alpha\beta n} = (-1)^n A_{\alpha\beta n}$, as do the expansion coefficients in Section C. This is necessary for consistency with the Onsager relation $\sigma_{\alpha\beta}(H) = \sigma_{\beta\alpha}(-H)$.

It is useful to list the conditions under which $\gamma_{\pm 1}$, $\gamma_1 \pm \gamma_{-1}$, and $\gamma_2 + \gamma_{-2}$ vanish by symmetry.

TABLE 1

Coefficient	Sufficient Condition
γ_1	1, 2 and 3, 4, 6
γ_{-1}	1, 2 and 3, 4, 5
$\gamma_1 + \gamma_{-1}$	1, 2, 4
$\gamma_1 - \gamma_{-1}$	1, 3, 4
$\gamma_2 + \gamma_{-2}$	5, 6, 4

Symmetries

1 z is a 2-fold axis

2 yz is a reflection plane

3 xz is a reflection plane

4 z is a 3- or 4-fold axis

5 x = y is a reflection plane

6 x = -y is a reflection plane

When H lies in a symmetry plane, and the conductivity tensor is resolved onto axes that also lie in symmetry directions, we therefore have considerable information already about the conductivity tensor, useful for checking numerical results. When $\sigma_{\alpha\beta}$ is written in the form

$$\sigma_{\alpha\beta} = \sigma_{\alpha\beta 0} + \sigma_{\alpha\beta 1} + \sigma_{\alpha\beta 2} \cdots \tag{I.34}$$

where $\sigma_{ijn} \propto H^{-n}$, we find that

$$\sigma_{xy1} = - \frac{e^2 k^3}{3\pi^2 m^* \omega} = - \frac{1}{\omega} \frac{Ne^2}{m^*} \tag{I.35}$$

is a constant independent of orientation, and that when H is along [001], [111], or [110] (in the last case, the axes on which $\sigma_{\alpha\beta}$ is resolved must be such that condition 5 or 6 holds), then $\gamma_{\pm 1} = \gamma_{\pm 2} = 0$ and so

$$\sigma_{xx2} = \sigma_{yy2} = \frac{e^2 k_F^2}{4\pi^2 m^* \omega^2} \int dk_z \sin^2\beta \; \frac{1}{\hat{\tau}}$$

$$= \frac{Ne^2}{m^*} \left\langle \frac{\bar{1}}{\tau} \right\rangle \frac{1}{\omega^2} \; . \tag{I.36}$$

Cubic symmetry was used in the last step. The bar denotes averaging within an orbit and the brackets averaging over all orbits. Finally we have

$$\sigma_{zz0} = \frac{e^2 k_F^2}{2\pi^2 m^*} \int dk_z \cos^2\beta\, \hat{\tau} = \frac{Ne^2}{m^*} \langle (\overline{\tau^{-1}})^{-1} \rangle \qquad \text{(I.37)}$$

This last average is quite different from the previous one, being weighted and dependent on the orientation of H. In the last line, the bar denotes averaging τ^{-1} over a single orbit, then the brackets denote averaging over all orbits the inverse of the inner average.

(I.35), (I.36), and possibly (I.37) are useful expressions because they can be calculated independently to confirm the numerical integration of (I.30).

When $\sigma_{\alpha\beta}$ is in the form of a power series, it can be inverted to find a similar expansion for $\rho_{\alpha\beta}$.

Zeroth Order

$$\rho_{xx0} = \frac{\sigma_{zz0}\sigma_{yy2} + \sigma_{yz1}^2}{\sigma_{zz0}\sigma_{xy1}^2}$$

$$\rho_{yy0} = \frac{\sigma_{zz0}\sigma_{xx2} + \sigma_{xz1}^2}{\sigma_{zz0}\sigma_{xy1}^2}$$

$$\rho_{zz0} = \frac{1}{\sigma_{zz0}} \qquad \text{(I.38)}$$

$$\rho_{xz0} = \rho_{zx0} = \frac{\sigma_{yz1}}{\sigma_{xy1}\sigma_{zz0}}$$

$$\rho_{yz0} = \rho_{zy0} = \frac{-\sigma_{xz1}}{\sigma_{xy1}\sigma_{zz0}}$$

$$\rho_{xy0} = \rho_{yx0} = 0 \quad .$$

First Order

$$\rho_{\alpha\alpha} = 0$$

$$\rho_{xy1} = -\rho_{yx1} = -\frac{1}{\sigma_{xy1}} = \frac{H}{Nec}$$

$$\rho_{xz1} = -\rho_{zx1} = \frac{\sigma_{xy1}\sigma_{yz2} + \sigma_{xy2}\sigma_{yz1} - \sigma_{yy2}\sigma_{xz1}}{\sigma_{xy1}^2\sigma_{zz0}}$$

$$\rho_{yz1} = -\rho_{zy1} = \frac{(-\sigma_{xy1}\sigma_{xz2} + \sigma_{xy2}\sigma_{xz1} - \sigma_{xx2}\sigma_{yz1})}{\sigma_{xy1}^2\sigma_{zz0}} .$$

Second Order

Let

$$\rho_{s2} = (\sigma_{xx2}\sigma_{yy2}\sigma_{zz0} + \sigma_{xx2}\sigma_{yz1}^2 - 2\sigma_{xy1}\sigma_{xz1}\sigma_{yz2}$$
$$+ 2\sigma_{xy1}\sigma_{xz2}\sigma_{yz1} - 2\sigma_{xy2}\sigma_{xz1}\sigma_{yz1}$$
$$+ \sigma_{xy1}^2\sigma_{zz2})/\sigma_{zz0}\sigma_{xy1}^2 .$$

Then

$$\rho_{xx2} = (\sigma_{yy4}\sigma_{zz0} + \sigma_{yy2}\sigma_{zz2} + 2\sigma_{yz1}\sigma_{yz3} -$$
$$- \sigma_{yz2}^2)/(\sigma_{zz0}\sigma_{yy2} + \sigma_{yz1}^2) - \rho_{s2} \quad . \quad \text{(I.39)}$$

cont'd.

$$\rho_{yy2} = (\underline{\sigma_{xx4}\sigma_{zz0}} + \sigma_{xx2}\sigma_{zz2} + 2\sigma_{xz1}\sigma_{xz3} -$$

$$- \sigma^2_{xz2})/(\underline{\sigma_{xx2}\sigma_{zz0}} + \sigma^2_{xz1}) - \rho_{s2}$$

$$\rho_{zz2} = (\underline{\sigma_{xx2}\sigma_{yy2}} - \sigma^2_{xy2} + 2\sigma_{xy1}\sigma_{xy3})/\underline{\sigma^2_{xy1}} - \underline{\rho_{s2}}$$

$$\rho_{xy2} = \rho_{yx2} = (-\sigma_{xz1}\sigma_{yz1} + \sigma_{xy2}\sigma_{zz0})/(\underline{\sigma^2_{xy1}\sigma_{zz0}}) \quad . \tag{I.39}$$

The underlined quantities are those that never vanish just as a consequence of symmetry. Terms of higher order were not calculated, because we already have the leading, and next to leading, terms of all components when H is away from symmetry directions. In symmetry directions, the longitudinal-transverse components (ρ_{xz}, ρ_{yz}, ρ_{zx}, and ρ_{zy}) vanish altogether (a situation that will be discussed later in this section) while for the transverse diagonal components, the saturated and first field dependent terms are already calculated.

Since the magnetic field modifies rather than cancels out the effect of the electric field on the electrons, an interesting quantity is the magnetoresistance

$$\Delta_{\alpha\alpha} \equiv \rho_{\alpha\alpha} - \frac{m^*}{Ne^2}\frac{1}{\langle\bar{\tau}\rangle} \quad . \tag{I.40}$$

the increase in the diagonal components of the resistivity tensor due to the magnetic field. That $\Delta_{\alpha\alpha}$ is strictly

greater than zero unless τ is isotropic, the F.S. spherical and the effective mass constant be proved from quite general principles [6], although this fact seems only very plausible from the following formulas for the saturation magnetoresistance

$$\Delta_{xx} = \left(\frac{\sigma_{zz0}\sigma_{yy2} + \sigma_{yz1}^2}{\sigma_{zz0}\sigma_{xy1}^2}\right) - \frac{m^*}{Ne^2}\frac{1}{\langle\bar{\tau}\rangle}$$

$$= \frac{m^*}{Ne^2}\left(\left\langle\frac{\bar{1}}{\tau}\right\rangle - \frac{1}{\langle\bar{\tau}\rangle}\right)$$

$$+ \frac{3m^*}{8Ne^2}\left\{\int d\beta \frac{\sin^3\beta}{\hat{\tau}}\left[(\gamma_2 + \gamma_{-2}) - (\gamma_1 + \gamma_{-1})^2\right]\right.$$

$$\left. + \left[\int d\beta \sin^2\beta\cos\beta(\gamma_1 + \gamma_{-1})\right]^2 / \int d\beta \sin\beta\cos^2\beta\hat{\tau}\right\} . \qquad \text{(I.41)}$$

Δ_{yy} is similar, but $(\gamma_2 + \gamma_{-2}) - (\gamma_1 + \gamma_{-1})^2$ is replaced by $-(\gamma_2 + \gamma_{-2}) + (\gamma_1 - \gamma_{-1})^2$, and in the quantity which is squared, $\gamma_1 + \gamma_{-1}$ by $i(\gamma_{-1} - \gamma_1)$.

The first term, the difference between those two averages, is the transverse magnetoresistance in the 3 principal symmetry directions (with certain qualifications for the [110] directions, see pg. 27). It can easily be proved positive definite, vanishing only for isotropic $\tau(\underline{k})$, and is a direct measure of the anisotropy of $\tau(\underline{k})$. The terms in curly brackets are less straightforward, but it seems plausible that the average of $-(\gamma_1 + \gamma_{-1})^2$ or $(\gamma_1 - \gamma_{-1})^2$, both strictly negative quantities, should be far

greater in magnitude than the square of the average of $\gamma_1 \pm \gamma_{-1}$, or the average of $\gamma_2 + \gamma_{-2}$. The result is that the transverse magnetoresistance reaches the same maximum value when H is along one of the 3 symmetry directions (usual qualifications on [110]) and decreases, never going below zero, away from them.

The saturation longitudinal magnetoresistance is very different.

$$\Delta_{zz} = \frac{m^*}{Ne^2} \left(\frac{1}{\langle \bar{\tau} \rangle} - \frac{1}{\langle (\overline{\tau^{-1}})^{-1} \rangle} \right) \qquad (I.42)$$

From (I.37) it is clear that the second average is actually weighted in favour of relaxation times at the poles. The poles, unlike the equator, sample only a few values of $\tau(\underline{k})$ (compare with (I.36)) and therefore such an average is sensitive to the direction of H. Δ_{zz} is therefore also a measure of anisotropy and we expect it to vary inversely with $\tau(0,0,k_F)$. A double application of the well-known inequality Average of $|f| \geq 1/\text{Average of } |1/f|$ shows that

$$\frac{1}{\langle \bar{\tau} \rangle} \frac{m^*}{Ne^2} \leq \rho_{zz0} \leq \frac{m^*}{Ne^2} \langle \frac{\bar{1}}{\tau} \rangle \quad , \qquad (I.43)$$

with equality holding only for isotropic $\tau(\underline{k})$. When $\tau(0,0,k_F)$ is approximately the same for two crystal orientations, other factors come into play. If $\tau(\underline{k})$ near the poles is almost independent of the azimuthal angle and depends largely on k_z, then ρ_{zz0} approaches the left hand side of inequality (I.43);

conversely if $\tau(\underline{k})$ near the poles is nearly independent of k_z and varies greatly only within a given orbit, ρ_{zz0} approaches the right side of (I.43). Therefore, the smaller value of ρ_{zz0} corresponds to the orientation for which any maxima or minima of $\tau(\underline{k})$ are more distant from and more symmetrically positioned about the poles.

The preceding arguments show that the transverse magnetoresistance as a function of orientation can be predicted from cubic symmetry alone, with only the depth and exact position of the minima being very complicated functions of $\tau(\underline{k})$. The longitudinal magnetoresistance is far more directly related to the particular $\tau(\underline{k})$ under consideration, and crystal symmetry plays only a secondary role.

(b) Intermediate Fields

This is where expansions in powers of H fail, since by definition intermediate fields are those where $\omega\langle\overline{\tau(\underline{k})}\rangle \sim 1$. We can still use the spherical symmetry of the F.S. and the cubic symmetry of $\tau(\underline{k})$ to reach the same conclusions as those deducible from Table 1 and (I.33) about the vanishing of the longitudinal transverse $\sigma_{\alpha\beta}$. For example, when z is a 2n-fold axis, $\gamma(\phi") = \gamma(\phi" + \pi)$, $v_y(\phi) = - v_y(\phi + \pi)$, $v_x(\phi) = - v_x(\phi + \pi)$, and all the quantities to the right of $v_x(\phi)$ in Eq. (I.30) are identical for ϕ and $\phi + \pi$; therefore, $\sigma_{xz}=\sigma_{yz}=0$. Similar arguments hold for a 3-fold axis, σ_{zx} and σ_{zy}.

It can also be shown that when xz is a reflection plane, $\sigma_{xz} = \sigma_{zx}$, $\sigma_{yz} = -\sigma_{yz}$ and $\sigma_{xy} = -\sigma_{yx}$, and conversely when yz is a reflection plane. But it is no longer true that σ_{xx} equals σ_{yy} when H is along [111], or that σ_{xx} is the same for H along [001] and [111]. Nevertheless, it seems plausible that the magnitude of the variations in the $\sigma_{\alpha\alpha}$ with the orientation of H should lie between those already described for the high and low field limits.

When not vanishing because of symmetry, the off-diagonal elements are proportional to H^n as $H \to 0$ and H^{-m} as $H \to \infty$ ($n>0$, $m \geq 0$); therefore, we expect these $\sigma_{\alpha\beta}$ to have maxima around $\omega\tau = 1$, unless of course they change sign there. If $\tau(\underline{k})$ were isotropic, there would only be one such maximum to consider (since the longitudinal-transverse components vanish), namely that of σ_{xy} which peaks at $\omega\tau = 1$ exactly. When $\tau(\underline{k})$ is anisotropic, different electrons satisfy this condition at different fields, therefore anisotropy should broaden this maximum. Quantities such as $\sigma_{\alpha\alpha}$, or other functions of the $\sigma_{\alpha\beta}$, which exhibit not a maximum but a "knee" near $\omega\langle\bar{\tau}\rangle = 1$, on log-log plots should also show a widening due to anisotropy of the transition region between high and low field behaviour. Except for σ_{xx} and σ_{yy} in symmetry directions, it is difficult to estimate the magnitude of this effect. The behaviour of σ_{xx} will be considered in more detail.

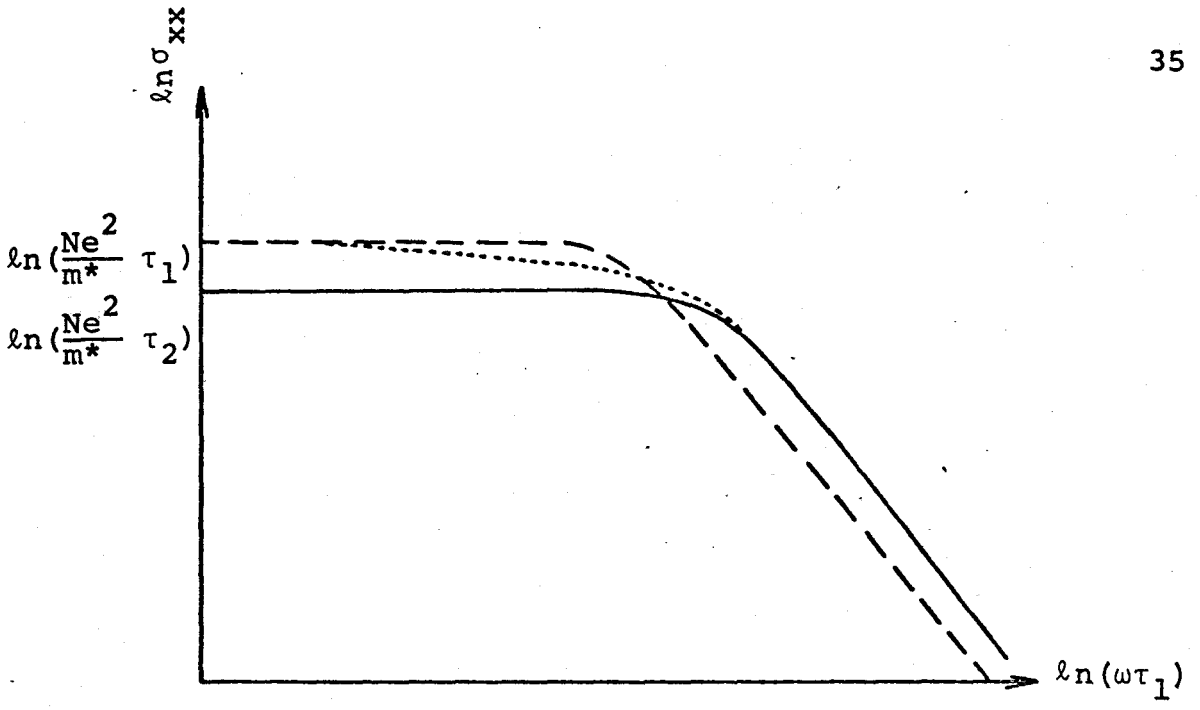

Fig. 2

----- $\tau(\underline{k}) = \tau_1 = \text{constant}$

——— $\tau(\underline{k}) = \tau_2 = \text{constant}$

····· $\tau(\underline{k})$ anisotropic

$\ell n\sigma_{xx}$ versus $\ell n(\omega\tau_1)$ at a constant temperature.

Let $\tau_1 = \langle\overline{\tau(\underline{k})}\rangle$, $\tau_2 = \langle\overline{\tau^{-1}(\underline{k})}\rangle^{-1}$ (note that $\tau_1 > \tau_2$).

Then

$$\lim_{H\to 0} \sigma_{xx} = \frac{Ne^2}{m^*}\tau_1 \quad \text{and} \quad \lim_{H\to\infty} \sigma_{xx} = \frac{Ne^2}{m^*}\frac{1}{\omega^2\tau_2} \ .$$

We can therefore sketch an envelope within which σ_{xx} (anisotropic) must lie (see Fig. 2). What we cannot guess is the factor by which σ_{xx} (anisotropic) has changed during the transition from high to low field behaviour. If this factor is much larger than τ_1/τ_2 then the broadening of the knee due to anisotropy will be a negligible effect.

Finally, we should note that when τ is isotropic, (I.30) can be easily integrated analytically to give

$$\begin{aligned} \sigma_{xx} &= \sigma_{yy} = \sigma_0/(1 + \omega^2\tau^2) \\ \sigma_{zz} &= \sigma_0 \\ \sigma_{xy} &= -\sigma_{yx} = -\sigma_0/(\omega\tau + \frac{1}{\omega\tau}) \end{aligned} \qquad \text{(I.44)}$$

and

$$\begin{aligned} \rho_{\alpha\alpha} &= 1/\sigma_0 \\ \rho_{xy} &= -\rho_{yx} = \frac{1}{\sigma_0}\omega\tau = \frac{H}{Nec} \ . \end{aligned} \qquad \text{(I.45)}$$

As foreseen there is no magnetoresistance.

(c) Justification for Some Approximations Made Earlier

When the effective mass (and therefore the cyclotron frequency ω) are not constant over the F.S., (I.30) must be written

$$\sigma_{\alpha\beta} = -\frac{e^2}{4\pi^3\hbar^2}\int_0^\infty \frac{\partial f_0}{\partial \varepsilon}\, d\varepsilon \int dk_z \frac{\overline{m^*(k_z)}}{\omega(k_z)} \frac{1}{1 - e^{-2\pi g}} \times \int_0^{2\pi} d\phi v_\alpha(\phi) \int_\phi^{2\pi+\phi} d\phi' v_\beta(\phi') \exp\{-g\int_\phi^{\phi'} \gamma(\phi'')d\phi''\} \qquad (I.46)$$

$\overline{m^*(k_z)}$ and $\omega(k_z)$ are the cyclotron mass and frequency for orbit k_z. $\overline{m^*(k_z)}$ is some sort of average of the effective masses in this orbit.

It is obvious that when the effective mass and F.S. radius are constant to within a few percent, $\tau(\underline{k})$ need only vary by 25% or so to dominate the $\Delta_{\alpha\alpha}$. For potassium, de Haas-van Alphen measurements [17] show that the areas of extremal orbits change by less than 1/500 with orientation. Experiments are accurate enough to allow contour maps [18] to be drawn showing how the radius of the F.S. varies on the irreducible 48th. In the [001] and [110] directions this radius is .15% and .1% larger than k_F, and in the [111] direction there is a -.1% depression. (k_F is the radius of a sphere with the volume enclosed by the F.S..)

Cyclotron resonance experiments indicate that the cyclotron mass for the equatorial (extremal) orbit is isotropic to within experimental error. This is consistent with calculations [19] suggesting that m* has about 2% anisotropy; $\overline{m^*(0)}$ samples points from all over the irreducible 48th and therefore should be far less anisotropic than m*. At first sight σ_{zz} appears to be proportional to $(\overline{m^*(k_F)})^2$, but this is not so; $\omega(k_z) \propto 1/(\overline{m^*(k_z)})$ and $v_\alpha = \hbar k_\alpha/m^*$, so that except at high fields where

$$(1 - e^{-2\pi g})^{-1} \approx \frac{\omega(k_z)\hat{\tau}}{2\pi} \propto \frac{\hat{\tau}}{\overline{m^*(k_z)}} \quad ,$$

σ_{zz} is just as insensitive to the anisotropy in m* as the other $\sigma_{\alpha\beta}$. Even then $\hat{\tau}(k_F)$ is about 200 times more anisotropic than $\overline{m^*(k_F)}$ at the temperature where our calculations are made. Therefore, it seems safe to assume isotropic m* and spherical F.S..

E. The Induced Torque

When a conducting material is placed in a time-varying magnetic field, eddy currents are set up in it which induce forces on the material. In the special case of a spherical conductor suspended from a wire in a magnetic field of constant magnitude whose direction rotates at constant frequency in the plane perpendicular to the wire, there exists an exact expression for the component of the induced torque parallel to the wire [7]

$$N_y = \frac{4\pi R^5 \Omega B^2}{15c^2} [(\text{trace } (\rho))I - \rho^t]^{-1}_{xx} \qquad (I.47)$$

R is the sample radius, Ω the angular frequency of rotation, B the field strength, I the unit 3×3 matrix, ρ and ρ^t the resistivity tensor and its transpose. ρ is resolved on axes with z parallel to B and y along the wire. An approximate expression which neglects the longitudinal-transverse terms of ρ but gives a better idea of the behaviour of N_y is

$$N_y \simeq \frac{4\pi R^5 \Omega B^2}{15c^2} \frac{\rho_{xx} + \rho_{zz}}{(\rho_{xx}+\rho_{zz})(\rho_{yy}+\rho_{zz}) - \rho_{xy}\rho_{yx}} . \qquad (I.48)$$

When $\rho_{xy} << \rho_{\alpha\alpha}$ (the low-field regime), another approximation can be made

$$N_y \simeq \frac{4\pi R^5 \Omega B^2}{15c^2} \frac{1}{\rho_{yy} + \rho_{zz}} \tag{I.49}$$

and when $\rho_{xy} >> \rho_{\alpha\alpha}$

$$N_y \simeq \frac{4\pi R^5 \Omega B^2}{15c^2} \frac{\rho_{xx} + \rho_{zz}}{|\rho_{xy}\rho_{yx}|} \tag{I.50}$$

$$\simeq \frac{4\pi R^5 \Omega}{15} (Ne)^2 (\rho_{xx} + \rho_{zz}) \quad . \tag{I.51}$$

In the intermediate case (equivalent to $\omega\langle\bar{\tau}\rangle = 1$), we have to go back to (I.48), or possibly (I.47) if the longitudinal-transverse components are relatively large. However, if we assume that ρ_{xy} is nearly constant and that Δ_{zz} is more sensitive to orientation than the transverse magnetoresistance, then (I.48) shows that the maxima of Δ_{zz} correspond to minima of N_y, just the opposite of the situation (I.5) where N_y is saturated.

Whereas the general form of the field dependence at constant temperature of N_y is easily seen from (I.50) and (I.51), the temperature dependence at constant field strength is a different matter because N_y is not just a function of the product $\omega\tau$. As long as $\omega\langle\bar{\tau}\rangle >> 1$, $N \propto \rho$ is an increasing function of temperature, but at sufficiently high temperatures $\omega\tau << 1$ and $N_y \propto \rho^{-1}$ starts to decrease down to zero.

Equation (I.50) is the main justification for developing this section. It shows that at saturation, just when the magnetoresistance and its sensitivity to crystal

orientation are greatest, the induced torque,which seems so indirect,is in fact very simply related to the magnetoresistance. Since measurements of the induced torque can be made without putting leads on the sample, (a great disadvantage in direct measurements of the resistivity) the induced torque method has at least one important experimental advantage in studies of the magnetoresistance.

CHAPTER II

METHOD

As was shown at the end of Section D, Eq. (I.30) may be integrated analytically for any field strength when $\tau(\underline{k})$ and m* are isotropic and F.S. is spherical. This suggests that each orbit might be subdivided into arcs on which $\tau(\underline{k})$ may be approximated by constants and analytic expressions, therefore, exist for the contribution from each arc to the partial conductivity $\frac{d\sigma_{ij}}{dk_z} \times dk_z$ due to the electrons in a particular orbit. However, from (I.30) it is clear that these contributions can simply be added when suitably weighted. If an orbit is cut in N arcs labelled by ℓ, and $\tau(\underline{k})$ = constant within each arc = τ_ℓ, and α_ℓ and β_ℓ are the initial and final values of ϕ, the angular variable, on arc ℓ, then

$$\frac{d\sigma_{\alpha\beta}}{dk_z} = \frac{m^* e^2}{4\pi^3 \hbar^2 \omega} \int dk_z (B^\alpha D^\beta + C^{\alpha\beta}) \qquad \text{(II.1)}$$

where

$$B^\alpha = \int_0^{2\pi} d\phi v_\alpha(\phi) \exp\{-\int_0^\phi \frac{d\phi''}{\omega\tau(\phi'', k_z)}\}$$
$$- \sum_{\ell=1}^{N} \exp\{-\frac{1}{\omega} \sum_{m=1}^{\ell-1} (\beta_m - \alpha_m) \frac{1}{\tau_m}\} \int_{\alpha_\ell}^{\beta_\ell} d\phi v_\alpha(\phi)$$
$$\times \exp(\frac{\alpha_\ell - \phi}{\omega\tau_\ell}) \qquad \text{(II.2)}$$

$$D^{\beta} = \int_0^{2\pi} d\phi v_{\beta}(\phi) \exp\{- \int_0^{2\pi} \frac{d\phi'}{\omega\tau(\phi')}\}$$

$$\times \left(1 - \exp\{- \int_0^{2\pi} \frac{d\phi'}{\omega\tau(\phi')}\}\right)^{-1}$$

$$= \sum_{\ell=1}^{N} \exp\{- \frac{1}{\omega} \sum_{m=\ell+1}^{N} (\beta_m - \alpha_m) \frac{1}{\tau_m}\}$$

$$\times \int_{\alpha_\ell}^{\beta_\ell} d\phi v_{\beta}(\phi) \exp\left(\frac{\phi - \beta_\ell}{\omega\tau_\ell}\right)$$

$$\times \left(1 - \exp\{- \frac{1}{\omega} \sum_{\ell=1}^{N} \frac{(\beta_\ell - \alpha_\ell)}{\tau_\ell}\}\right)^{-1} \qquad \text{(II.3)}$$

$$C^{\alpha\beta} = \int_0^{2\pi} d\phi \int_0^{\phi} d\phi' v_{\alpha}(\phi) v_{\beta}(\phi') \exp\{- \int_{\phi}^{\phi} \frac{d\phi''}{\omega\tau(\phi'')}\}$$

$$= \sum_{m=1}^{N} \Big[\int_{\alpha_m}^{\beta_m} d\phi \int_{\alpha_m}^{\phi} d\phi' v_{\alpha}(\phi) v_{\beta}(\phi') \exp\left(\frac{\phi' - \phi}{\omega\tau_m}\right)$$

$$+ \int_{\alpha_m}^{\beta_m} d\phi v_{\alpha}(\phi) \exp\left(\frac{\alpha_m - \phi}{\omega\tau_m}\right)$$

$$\times \sum_{\ell=1}^{m-1} \exp\{- \frac{1}{\omega} \sum_{n=\ell+1}^{m-1} \frac{(\beta_n - \alpha_n)}{\tau_n}\}$$

$$\times \int_{\alpha_\ell}^{\beta_\ell} d\phi' v_{\beta}(\phi') \exp\left(\frac{\phi' - \beta_\ell}{\omega\tau_\ell}\right) \Big] \quad . \qquad \text{(II.4)}$$

Analytic expressions exist for all the integrals appearing in (II.2), (II.3), and (II.4). With a computer it is simple in principle to evaluate these expressions, compute the sums in (II.2), (II.3), and (II.4), and then sum (II.1) over orbits. This was first done by Douglas and

Datars [9] for aluminum. Once $\tau(\underline{k})$ is known, the only remaining problem is the subdivision of the orbits into arcs and the choice of intervals Δk_z between orbits. At first the τ_ℓ were determined by reducing the wavevector corresponding to the middle of arc ℓ to the irreducible 48th, determining which of the 21 points where $\tau(\underline{k})$ had been calculated lay closest, and assigning that value to τ_ℓ; but this method was abandoned because it generated absurdly large values for the off-diagonal conductivity tensor components in the low-field limit. It was equivalent to having discontinuous $\tau(\underline{k})$, an unphysical situation which not surprisingly led to trouble when integrals over derivatives of $\tau(\underline{k})$ were evaluated - in (I.16) for example, the cancellation of the derivatives, required by cubic symmetry, did not take place. Since the low-field Hall coefficient can be calculated without the use of a path-integral, and the diagonal components of $\rho_{\alpha\beta}$ are barely different from the zero-field values, such a problem in the low-field limit would seen not to matter; unfortunately at intermediate fields, where there is no alternative to the path-integral, this problem can be expected to persist. For this reason the τ_ℓ were determined by evaluating a continuous and smooth function having cubic symmetry in the middle of arc ℓ. It was ascertained that the function had no unwanted small wriggles between the 21 points because the derivatives of τ would pick them up; as far as the high-field limit was concerned, it was good enough

if the function had the right shape only on the average, because those low Fourier coefficients $\gamma_{\pm 1}$ and $\gamma_{\pm 2}$ are sensitive only to the larger features of $\tau(\underline{k})$. The function used was a good fit to the 21 given values; at 4K for the pure metal it differed by at most 6% from the given values, and the fit improved as the scattering times became more isotropic.

A total of 93 orbits were summed over. The interval Δk_z decreased from a maximum value of $\frac{k_F}{50}$ at the equator as the orbits grew smaller. The arcs in a given orbit were of equal length, approximately $k_F/30$ (an interval over which $\tau(\underline{k})$ changes by at most 13%) and the number of arcs was always a multiple of 12, to make sure that the program detected 3- or 4-fold symmetry (if any) about the z axis. It was found that in the high-field limit ($\omega\langle\bar{\tau}\rangle = 3 \times 10^3$) reducing both the arc length and Δk_z by a factor of 2 caused a change in the $\Delta_{\alpha\alpha}$ of less than .1%, in σ_{xy} of .003%, and in the longitudinal-transverse $\rho_{\alpha\beta}$ of about 1%.

Equations (I.19), (I.33), and Table 1 imply a large number of tests for inconsistencies in the program. There is no doubt that it passes all of them, and is in fact extremely accurate. For example, $H \times \sigma_{xy}$, a constant in the high-field limit depending only on the volume of the F.S., is calculated by the program with an error of .005%; ρ_{xx} and ρ_{yy} which should be equal and have the same value when $\underline{H}$ is along

[001] and [111] when $\omega\langle\overline{\tau(\underline{k})}\rangle >> 1$ differ by .005%. Since the program samples $\tau(\underline{k})$ at about 9000 points on $\frac{1}{2}$ the F.S., it can easily compute $\frac{m^*}{Ne^2}\langle\overline{\tau(k)^{-1}}\rangle$ for comparison with ρ_{xx} when $\underline{H}$ lies along [001] or [111]; the difference is .005%. In fact, for self-consistency, the program calculates the zero-field resistivity $\frac{m^*}{Ne^2}\frac{1}{\langle\overline{\tau(k)}\rangle} \equiv \rho_0$ which it subtracts from the $\rho_{\alpha\alpha}$ to obtain the $\Delta_{\alpha\alpha}$ in just this way. However, the values of $\langle\overline{\tau(\underline{k})}\rangle^2$ and $\langle\overline{\tau^2(\underline{k})}\rangle$ which were used to plot Fig. 7 did come directly from the 21 points. The induced torque was computed using the exact expression (I.47), not (I.48).

CHAPTER III

RESULTS AND DISCUSSION

The conductivity tensor and the quantities derivable from it were computed as functions of temperature, magnetic field strength and orientation for potassium with several different residual resistivities. The results are shown in Figs. 3 to 21.

(a) The Temperature Dependence

Figure 3 shows Δ_{xx} for various impurity concentrations and magnetic field strengths. The fields were chosen so that for the larger value, $\omega\langle\tau(\underline{k})\rangle$ was much greater than unity over the entire temperature range shown; for the smaller value, $\omega\langle\bar{\tau}\rangle$ ranged from 3000 to .03, reaching a value of 35 at 4K. At 8K (where $\omega\langle\tau(\underline{k})\rangle \sim 1$) the curve belonging to the smaller field strength slips below the others because for a given temperature Δ_{xx} is a strictly decreasing function of H [6].

Figure 3 may be compared with Fig. 4 showing experimental results [10]. The calculated Δ_{xx} are smaller by a factor of 7, probably because the observations were made at fields high enough that the linear increase in the magneto-resistance (described later) made the measured Δ_{xx} anomalously

Fig. 3: $H = 1.2 \times 10^4$ k0e

- ——— $\rho_{res} = 0$
- ····· $\rho_{res} = 10^{-4}$ μ-ohm-cm
- ----- $\rho_{res} = 10^{-3}$ "

$H = 1.2$ k0e -·-·- $\rho_{res} = 0$

H is along [001], y along [010].

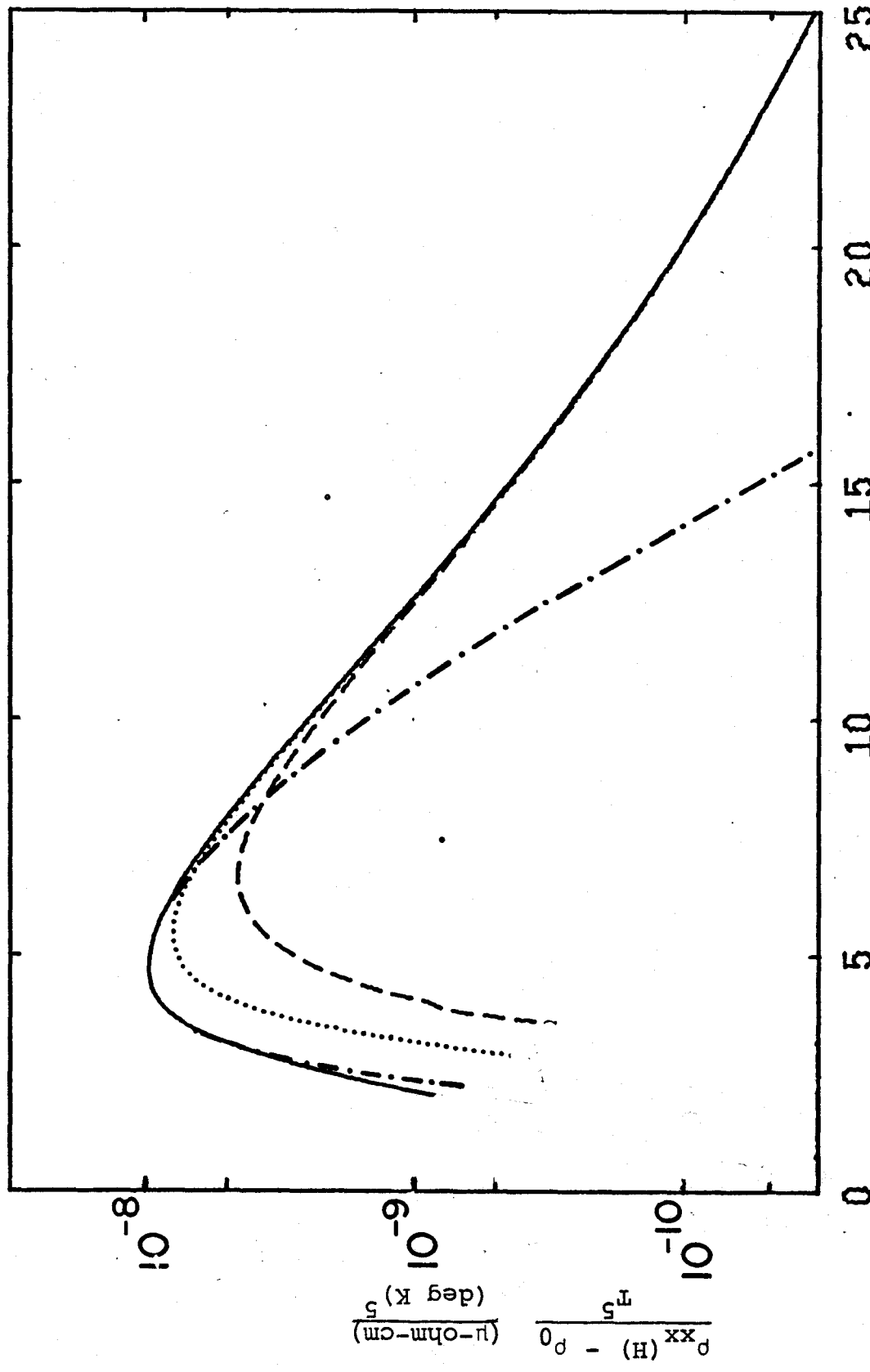
10^{-8}
10^{-9}
10^{-10}
$\frac{\rho_{xx}(H) - \rho_0}{T^5}$
$\frac{(\mu\text{-ohm-cm})}{(\text{deg K})^5}$
0
5
10
15
20
25
T(°K)

Fig. 3

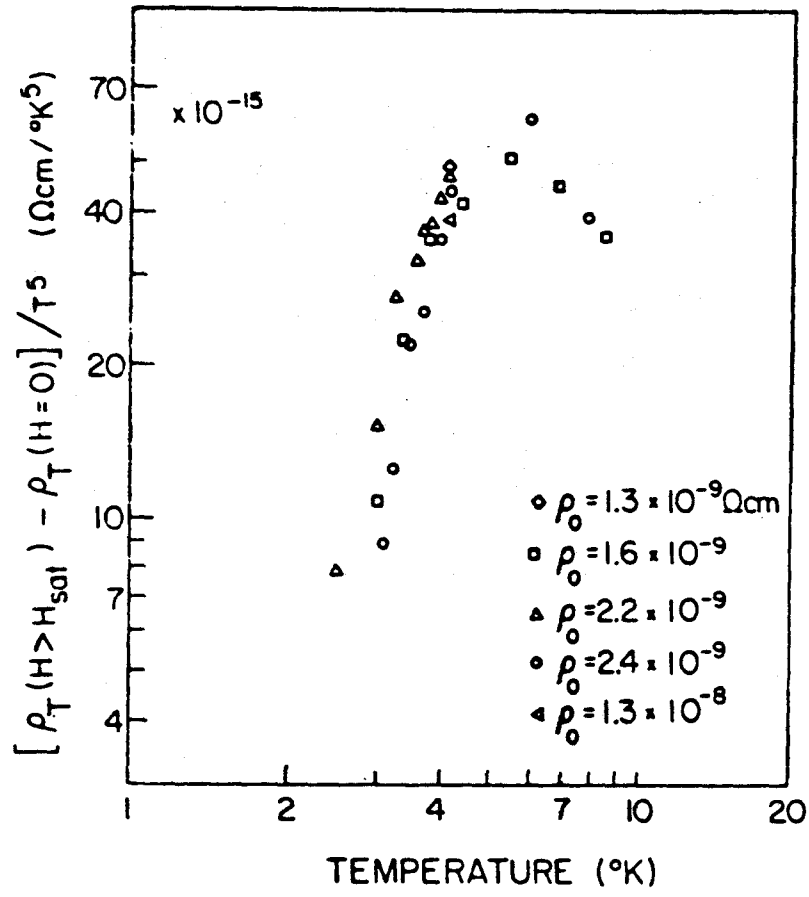

FIG. 4: Observed change in the intrinsic resistivity of potassium resulting from the application of a large transverse magnetic field; as measured by Babiskin and Siebenmann, Ref. 10. (H_{sat} is the field at which the phonon component of the magnetoresistivity saturates, see text.)

large. The general shape of the curve seems about right, though.

Figures 5 and 6 illustrate the temperature dependence of the specific induced torque discussed in Section E for two different field strengths.

Figure 7 shows the temperature dependence of $\langle\overline{\tau(\underline{k})}\rangle^2/\langle\overline{\tau^2(\underline{k})}\rangle$ as calculated by Hayman and Carbotte [24], which is inversely proportional to the low-field Hall coefficient.

Figure 8 shows the relative magnitudes of various components of the conductivity at 4K over a wide range of fields. Their linear or quadratic dependence in the limiting cases on the field is apparent from this plot. By comparison the resistivity tensor displays less variety - on the scale used in Fig. 8 the $\rho_{\alpha\alpha}$ would appear as horizontal lines, ρ_{xy} as a straight line whose slope changes imperceptibly by a factor of $\langle\overline{\tau^2}\rangle/\langle\overline{\tau}\rangle^2$ from one end of the plot to the other; only the longitudinal-transverse components would show interesting behaviour, either saturating or decreasing as H^{-2}. The saturation value of these components, if any, is about twice the value at $\omega\langle\overline{\tau(\underline{k})}\rangle \sim 1$.

Figures 9 and 10 show how anisotropy of scattering time blurs the transition region between high and low field limits. In Fig. 10 the curves meet asymptotically at the left, and off the right side of the graph eventually run parallel and slightly separated; in Fig. 11 the reverse holds true. The predicted effects exist, but they are negligibly

Fig. 5: Specific induced torque versus temperature for $H = 1.2 \times 10^4$ kOe. $\underline{H}$ is along [001].

Fig. 6: Specific induced torque versus temperature for $H = 1.2$ kOe. $\underline{H}$ is along [001].

Fig. 5

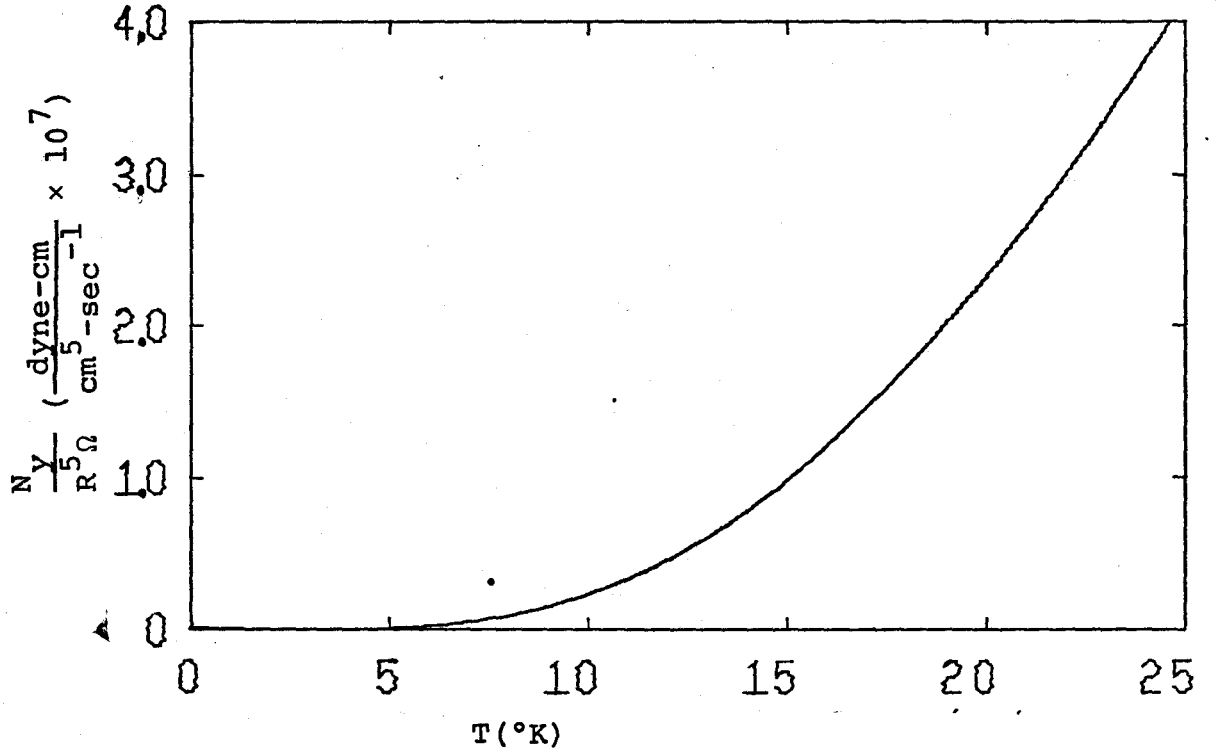
4.0
3.0
2.0
1.0
0
0
5
10
15
20
25
T(°K)
$\frac{N_y}{R^5\Omega}$ ($\frac{\text{dyne-cm}}{\text{cm}^5\text{-sec}^{-1}} \times 10^7$)

Fig. 6

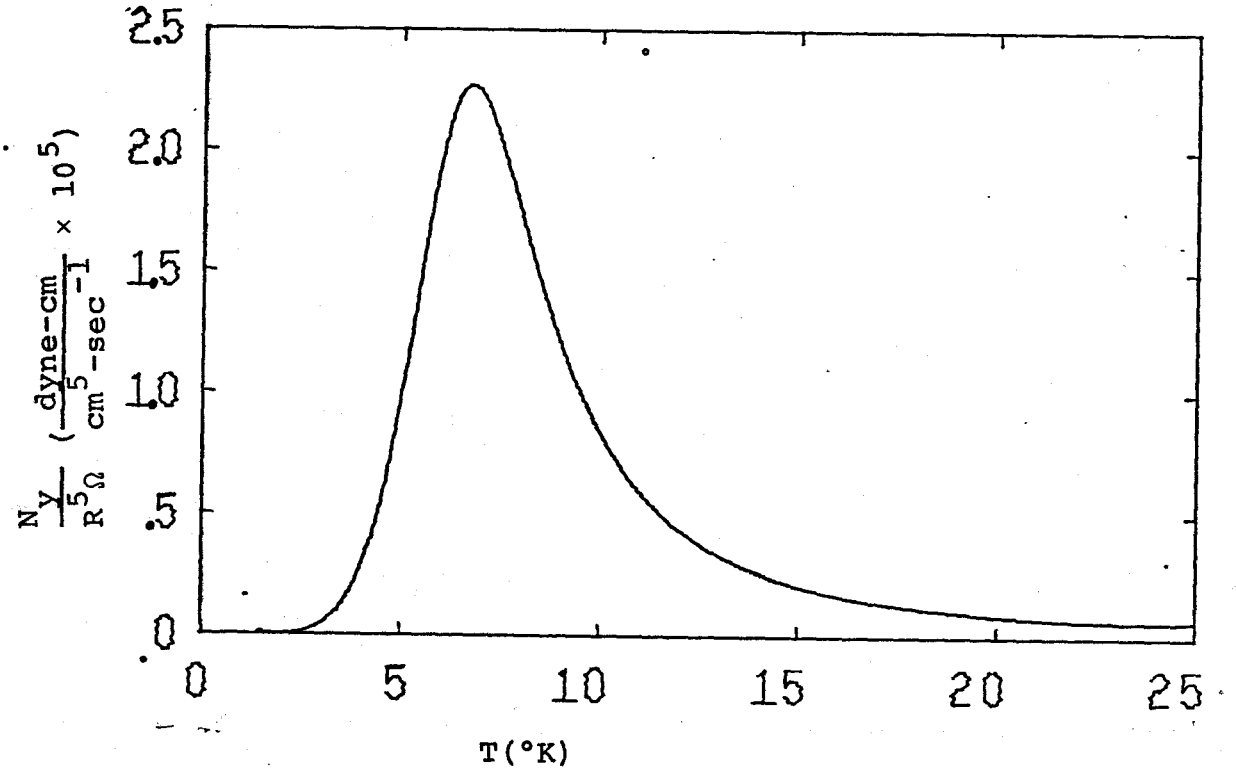
2.5
2.0
1.5
1.0
.5
0
0
5
10
15
20
25
T(°K)
$\frac{N_y}{R^5\Omega}$ ($\frac{\text{dyne-cm}}{\text{cm}^5\text{-sec}^{-1}} \times 10^5$)

Fig. 7: $\langle\overline{\tau(\underline{k})}\rangle^2/\langle\overline{\tau^2(\underline{k})}\rangle$ as a function of temperature for the same pseudopotentials as listed in Fig. 1. The upper curve corresponds to the $\tau(\underline{k})$ actually used in our calculations.

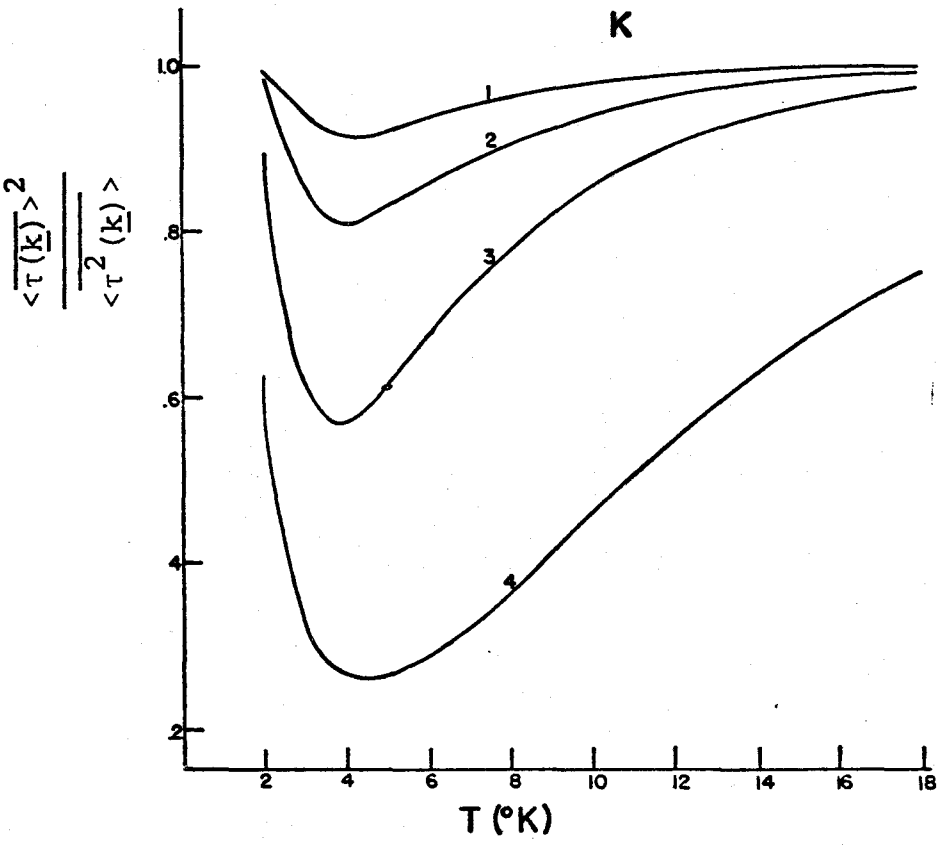

Fig. 7

As calculated by Hayman and Carbotte [24].

Fig. 8: ——— σ_{xx}, σ_{yy} T = 4K, ρ_{res} = 0.
····· $|\sigma_{xy}|$ · $\underline{H}$ in the [010] plane
----- $|\sigma_{xz}|$ 20° from [001] towards
-·-· $|\sigma_{yz}|$ [101], y along [010].
-···- σ_{zz}

Fig. 9: Comparison of σ_{xx} for $\tau(\underline{k})$ anisotropic (T = 4K and ρ_{res} = 0) and $\tau(\underline{k})$ isotropic (= $\langle\overline{\tau(\underline{k})}\rangle$). $\underline{H}$ is along [001], y along [010].

Fig. 8

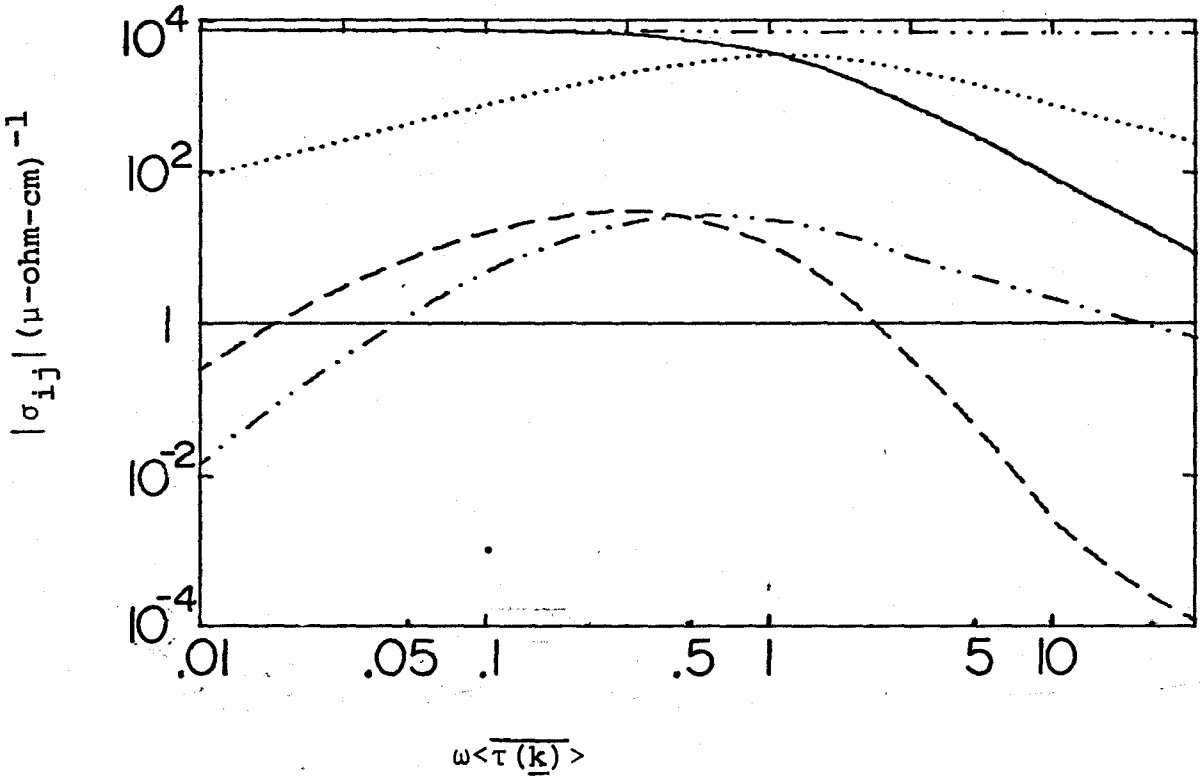
10^4
10^2
1
10^{-2}
10^{-4}
.01
.05
.1
.5
1
5
10
$|\sigma_{ij}|$ (μ-ohm-cm)$^{-1}$
$\omega\langle\overline{\tau(\underline{k})}\rangle$

Fig. 9

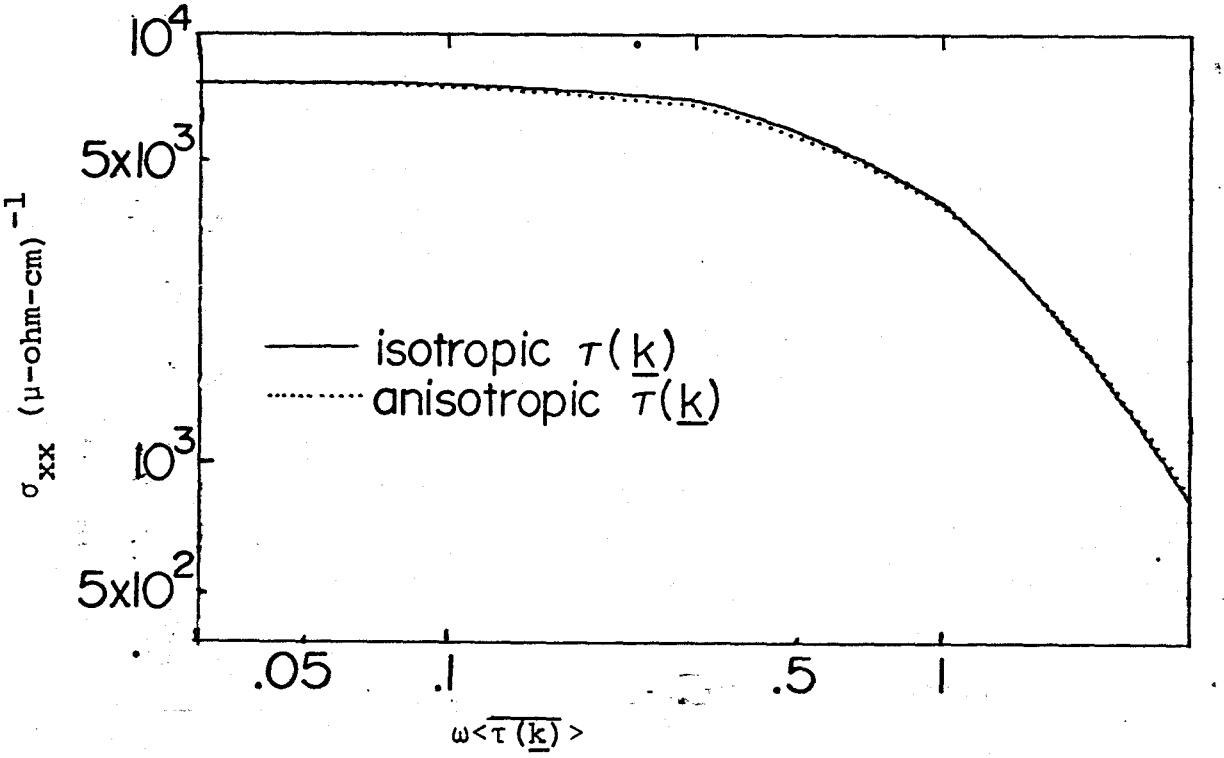
10^4
5×10^3
10^3
5×10^2
isotropic $\tau(\underline{k})$
anisotropic $\tau(\underline{k})$
.05
.1
.5
1
σ_{xx} (μ-ohm-cm)$^{-1}$
$\omega\langle\overline{\tau(\underline{k})}\rangle$

Fig. 10: Comparison of σ_{xy} for isotropic τ ($= \langle\tau(\underline{k})\rangle$) and anisotropic $\tau(\underline{k})$ ($\rho_{res} = 0$, T = 4K). $\underline{H}$ is along [001], y along [010].

Fig. 11: Induced torque plotted as a function of field strength; T = 4K, $\rho_{res} = 0$. $\underline{H}$ is along [001], y along [010].

Fig. 10

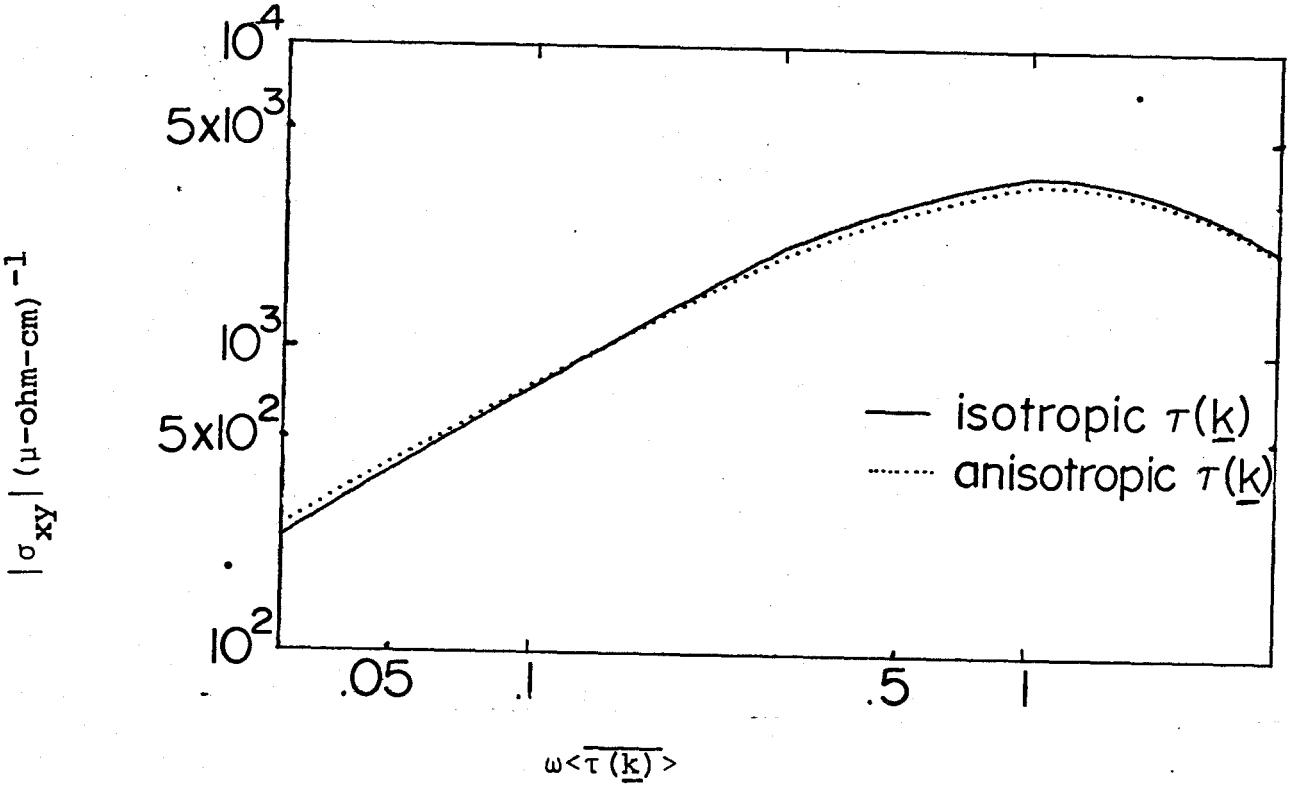
10^4
5×10^3
10^3
5×10^2
10^2
.05
.1
.5
1
isotropic $\tau(\underline{k})$
anisotropic $\tau(\underline{k})$
$|\sigma_{xy}|$ (μ-ohm-cm)$^{-1}$
$\omega\langle\overline{\tau(\underline{k})}\rangle$

Fig. 11

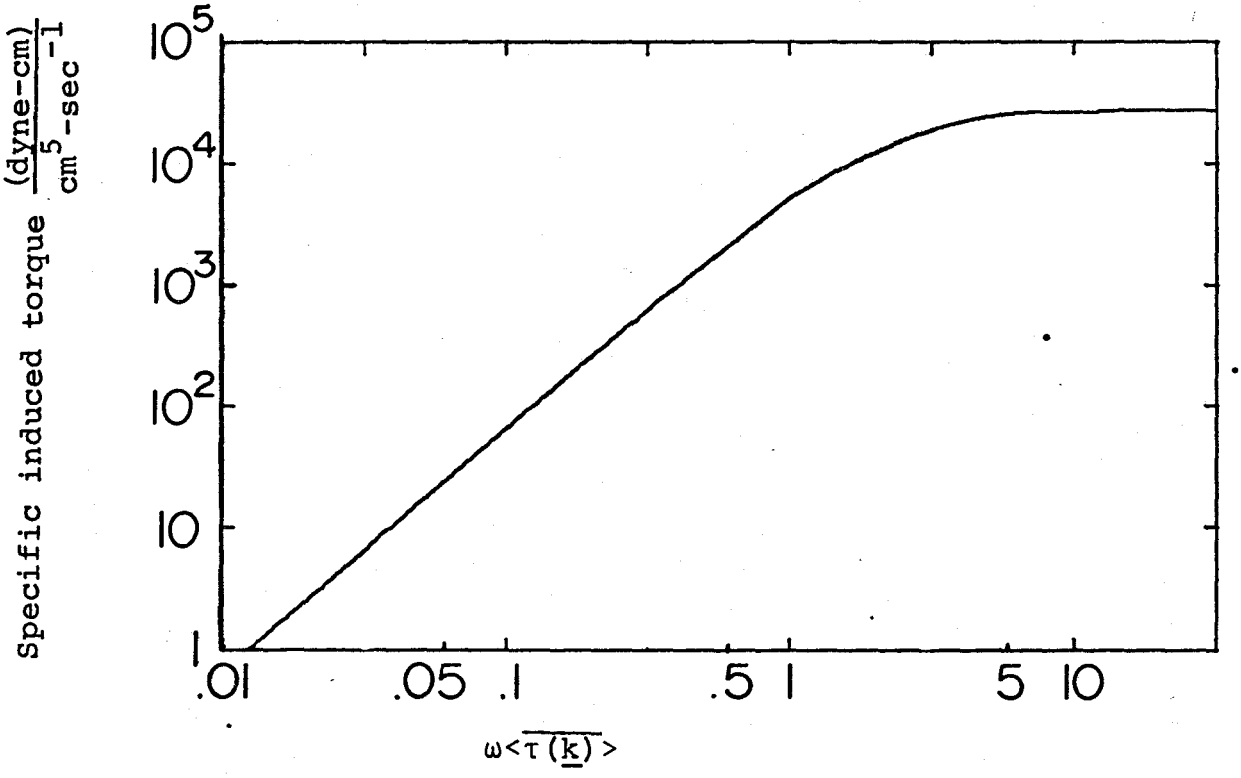
10^5
10^4
10^3
10^2
10
1
.01
.05
.1
.5
1
5
10
Specific induced torque $\frac{(\text{dyne-cm})}{\text{cm}^5\text{-sec}^{-1}}$
$\omega\langle\overline{\tau(\underline{k})}\rangle$

small. In Fig. 7, which shows the field dependence of the specific induced torque, such effects are simply not noticeable.

The remaining graphs illustrate the effects of rotating the magnetic field with respect to the crystal axes. It is important to keep in mind that the axes on which $\sigma_{\alpha\beta}$ was resolved rotate with the field, according to the convention described earlier. Only the y axis always maintains the same orientation with respect to the crystal, a different orientation in the 3 sections of each graph. This geometry was chosen with induced torque in mind. Two field strengths were chosen, such that $\omega\langle\overline{\tau(\underline{k})}\rangle \sim 1$ and $\omega\langle\overline{\tau(\underline{k})}\rangle \sim 3000$ (At 4K, $\langle\overline{\tau_0(\underline{k})}\rangle \simeq 2 \times 10^{-9}$ sec^{-1}.) The latter value ensures that N_y and $\Delta_{\alpha\alpha}$ reach their saturation values - any further increase in the field strength caused changes of about 1 part in 10^8 in the $\rho_{\alpha\alpha}$. A third value, $\omega\langle\overline{\tau(\underline{k})}\rangle \sim .05$ was partly computed and not shown because the $\Delta_{\alpha\alpha}$ were so small (.03% of ρ_0); $\Delta_{\alpha\alpha}$ decreases very rapidly for $\omega\langle\overline{\tau(\underline{k})}\rangle$ less than unity.

Results are shown mostly for the pure metal at 4K. The choice of $\rho_{res} = 10^{-4}$ μ-ohm-cms reduced the ratio of $\tau(001):\tau(111)$ from 4:1 to 2:1, but also reduced $\langle\overline{\tau(\underline{k})}\rangle$ so that the magnitudes of the Δ_{xx} were only reduced by a factor of 2 although Δ_{zz}/ρ_0 was reduced by a factor of 3.5.

Two plots of variations in the $\sigma_{\alpha\alpha}$ (Figs. 12 and 13) are shown, mainly because the $\sigma_{\alpha\alpha}$ are more simply described

Fig. 12: ——— xx $\omega\langle\overline{\tau(\underline{k})}\rangle \sim 3 \times 10^3$

····· yy

----- zz $T = 4K$, $\rho_{res} = 0$

Diagonal components of conductivity tensor versus orientation of field.

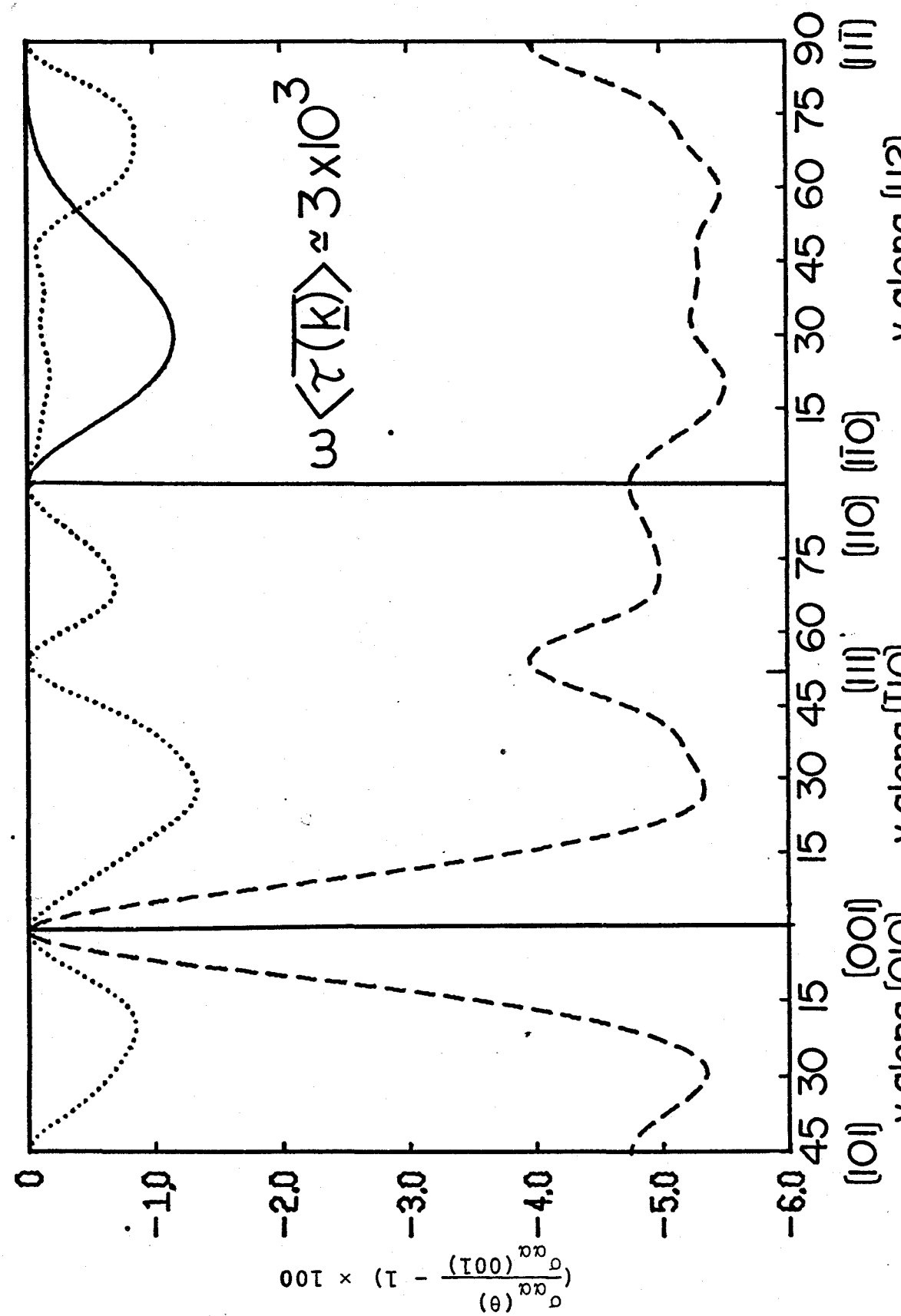
$\omega\langle\tau(\underline{k})\rangle \simeq 3\times10^{3}$
$\frac{(\sigma_{\alpha\alpha}(\theta)}{\sigma_{\alpha\alpha}(001)} - 1) \times 100$
0
-1.0
-2.0
-3.0
-4.0
-5.0
-6.0
45 30 15
[101]
y along [010]
[001]
15 30 45 60 75
y along [$\bar{1}$10]
[111]
[110]
15 30 45 60 75 90
y along [112]
[$\bar{1}$11]
[$\bar{1}$10]

Fig. 12

Fig. 13: ——— xx $T = 4K$, $\rho_{res} = 0$

····· yy

----- zz $\omega\langle\overline{\tau(\underline{k})}\rangle \sim 1$

Conductivity tensor versus field orientation.

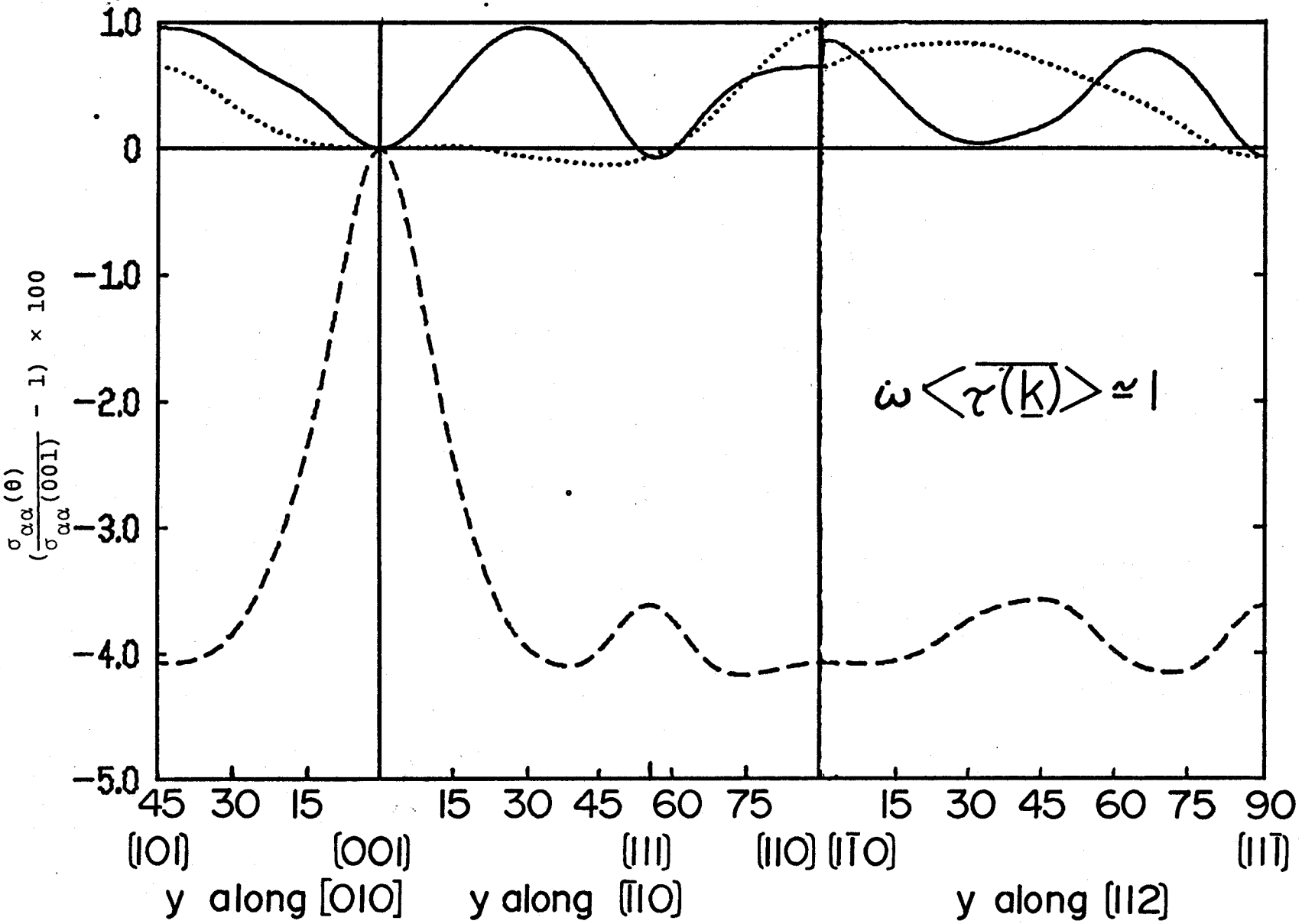
1.0
0
−1.0
−2.0
−3.0
−4.0
−5.0
$\left(\frac{\sigma_{\alpha\alpha}(\theta)}{\sigma_{\alpha\alpha}(001)} - 1\right) \times 100$
$\omega\langle\overline{\tau(\underline{k})}\rangle \simeq 1$
45 30 15
15 30 45 60 75
15 30 45 60 75 90
[101]
[001]
[111]
[110]
[1$\bar{1}$0]
[11$\bar{1}$]
y along [010]
y along [$\bar{1}$10]
y along [112]

Fig. 13

in terms of the expansion coefficients (I.33). In Fig. 12 the fact that $\sigma_{xx}(001) = \sigma_{xx}(101) \simeq \sigma_{xx}(110)$ shows that the quadratic term in $\gamma_{\pm 1}$ and not $\gamma_2 + \gamma_{-2}$ is responsible for the bumps in the transverse conductivities, since $\gamma_2 + \gamma_{-2}$ is in general non-vanishing for the [110] direction. In the first two segments of the plot, σ_{xx} is constant because y lies in a symmetry direction, but when y is along [112] this symmetry is broken.

Figure 14 shows the longitudinal-transverse $\rho_{\alpha\beta}$ for the two fields. Again, symmetry apparently causes the high-field ρ_{yz} to vanish when y is not along [112], but examination of (I.33) shows it is even and non-zero but much smaller than ρ_{xz} which is always odd. (When y does lie along [112] ρ_{yz} is also odd.) When $\omega\langle\overline{\tau(\underline{k})}\rangle \sim 1$, ρ_{xz} and ρ_{yz} have grown to about the same size, vanishing (totally, not approximately) when z lies along an n-fold axis. In the first two sections of the graph, ρ_{xz} was even and ρ_{yz} odd; in the last section, both were even but only approximately so. The maximum value of the longitudinal-transverse $\rho_{\alpha\beta}$ was about $\rho_0/200$.

The Hall coefficient, $(\equiv \frac{\rho_{yx} - \rho_{xy}}{2H})$, is independent of orientation in the limiting cases, but displays some anisotropy at intermediate dields (Fig. 15). (I.40) and (I.20) show how anisotropy in ρ_{xy} and ρ_{yx} begins to develop in the limiting cases. In the first two sections of the graph $\rho_{xy} = -\rho_{yx}$ because the xz plane is a reflection plane.

Fig. 14: ——— ρ_{xz} } $\omega\langle\overline{\tau(\underline{k})}\rangle \sim 1$
..... ρ_{yz} }

----- ρ_{xz} } $\omega\langle\overline{\tau(\underline{k})}\rangle \sim 3 \times 10^3$
-.-.- ρ_{yz} }

Longitudinal-transverse components of the resistivity tensor for T = 4K and $\rho_{res} = 0$.

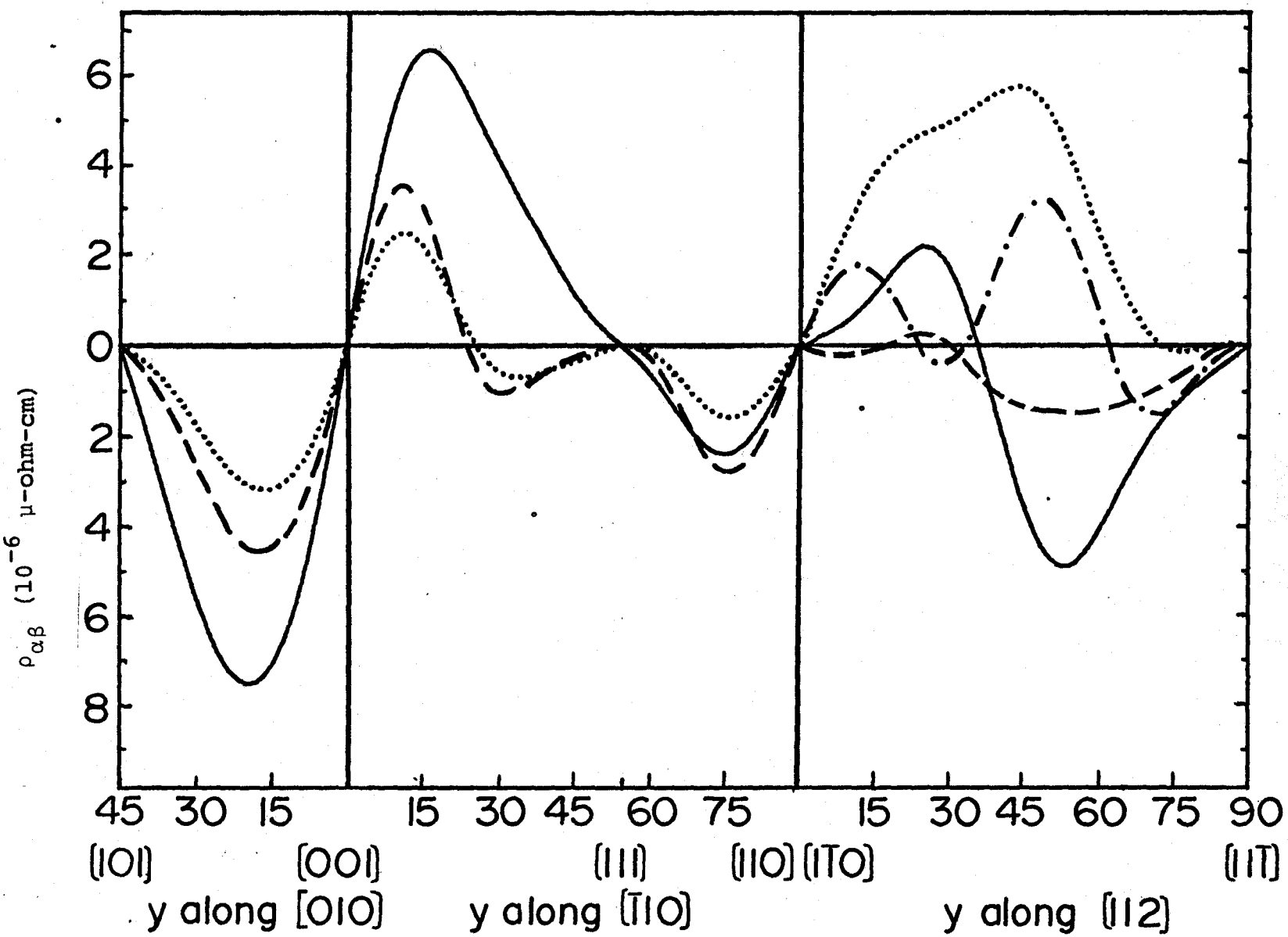
6
4
2
0
2
4
6
8
$\rho_{\alpha\beta}$ (10^{-6} μ-ohm-cm)
45 30 15
15 30 45 60 75
15 30 45 60 75 90
[101]
[001]
[111]
[110]
[1T0]
[11T]
y along [010]
y along [T10]
y along [112]

Fig. 14

Fig. 15: ——— $\dfrac{\rho_{xy}(\theta)}{\rho_{xy}(001)} - 1 = \Delta\rho_{xy}$

····· $\dfrac{-\rho_{yx}(\theta)}{\rho_{yx}(001)} + 1 = \Delta\rho_{yx}$

----- $\dfrac{R_H(\theta)}{R_H(001)} - 1 = \Delta R_H$

Anisotropy of ρ_{xy}, ρ_{yx} and the Hall coefficient $R_H \equiv (\rho_{yx} - \rho_{xy})/2H$ when $\omega\langle\overline{\tau(\underline{k})}\rangle \sim 1$. In the first two parts of the graph, the dashed and dotted curves coincide.

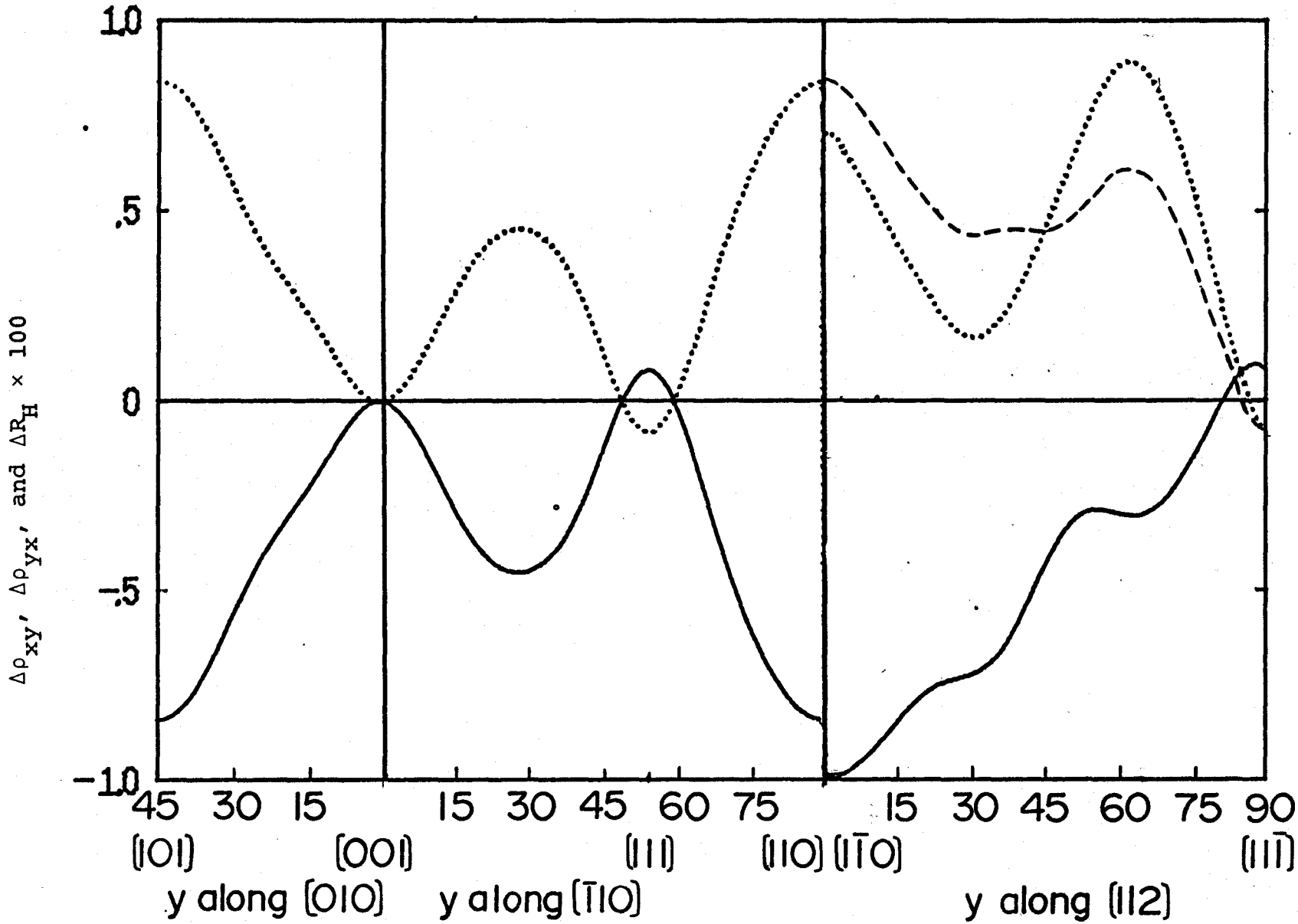
1.0
.5
0
-.5
-1.0
$\Delta\rho_{xy}$, $\Delta\rho_{yx}$, and $\Delta R_H \times 100$
45 30 15
15 30 45 60 75
15 30 45 60 75 90
[101]
[001]
[111]
[110]
[1$\bar{1}$0]
[11$\bar{1}$]
y along [010]
y along [$\bar{1}$10]
y along [112]

Fig. 15

The $\Delta_{\alpha\alpha}/\rho_0$ shown in the next 3 plots are believed to be underestimates. It is difficult to say by how much; however, comparison of the cases $\rho_{res} = 0$ and $\rho_{res} = 10^{-4}$ and Fig. 3 suggests that Δ_{ii}/ρ_0 is a non-linear and rapidly increasing function of $\tau(001)/\tau(111)$. The predicted variations in the $\Delta_{\alpha\alpha}$ are well within the accuracy with which the resistivity of potassium has been measured in the absence of a magnetic field ($\pm$ 2 $\times$ 10^{-7} μ-ohm-cm) [12], but difficulties with the leads make it hard to use the 4-probe method to measure $\Delta_{\alpha\alpha}$ directly for the same sample at different orientations. In symmetry directions, where comparisons with $\langle\overline{\tau^{-1}(\underline{k})}\rangle$ can be made, the $\Delta_{\alpha\alpha}$ are calculated to within .3% by the path-integral, therefore, even the finer features of the curves shown are believed to be significant.

According to (I.38), the magnetoresistance should saturate at high fields. Experiments strongly suggest [13] that it does not - it shows a slow linear increase with H even at very high [21] fields. In a simple metal like potassium it is difficult to see where the anomaly comes from. Local "hot spots" on the F.S. where $\omega\tau(\underline{k})$ is still < 1 at very high fields [22], charge density waves [20] and effects peculiar to polycrystalline samples [10], have all been proposed as explanations, but there is still no agreement on the cause of the linear magnetoresistance.

There is some experimental evidence for magnetoresistance anisotropy in potassium. Simpson [23] using the

Fig. 16: ——— xx $T = 4K$, $\rho_{res} = 0$

····· yy

----- zz $\omega\langle\overline{\tau(\underline{k})}\rangle \sim 3 \times 10^3$

$\frac{\Delta_{\alpha\alpha}}{\rho_0}$ as a function of orientation.

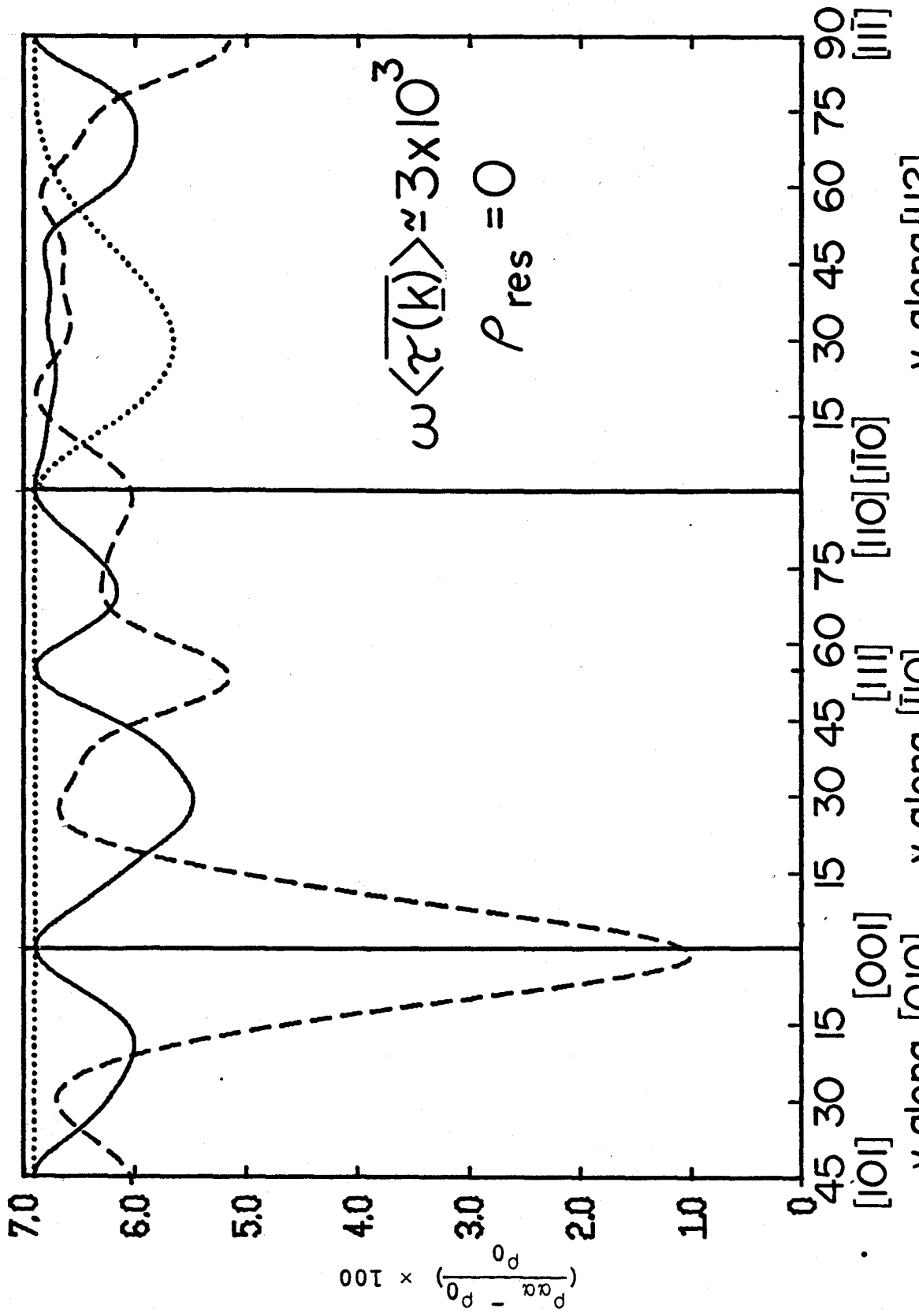
$\omega\langle\overline{\tau(\underline{k})}\rangle \simeq 3\times10^{3}$
$\rho_{res} = 0$
$\frac{(\rho_{\alpha\alpha} - \rho_0)}{\rho_0} \times 100$
7.0
6.0
5.0
4.0
3.0
2.0
1.0
0
45 30 15 [001] 15 30 45 60 75 [111] 75 [110] [1$\bar{1}$0] 15 30 45 60 75 90 [111]
y along [$\bar{1}$01]
y along [010]
y along [$\bar{1}$10]
y along [$\bar{1}$10]
y along [112]

Fig. 16

Fig. 17: ——— xx $T = 4K$, $\rho_{res} = 10^{-4}$ μ-ohm-cm

····· yy

----- zz $\omega\langle\bar{\tau}(\underline{k})\rangle \sim 3 \times 10^3$

$\frac{\Delta_{\alpha\alpha}}{\rho_0}$ as a function of orientation.

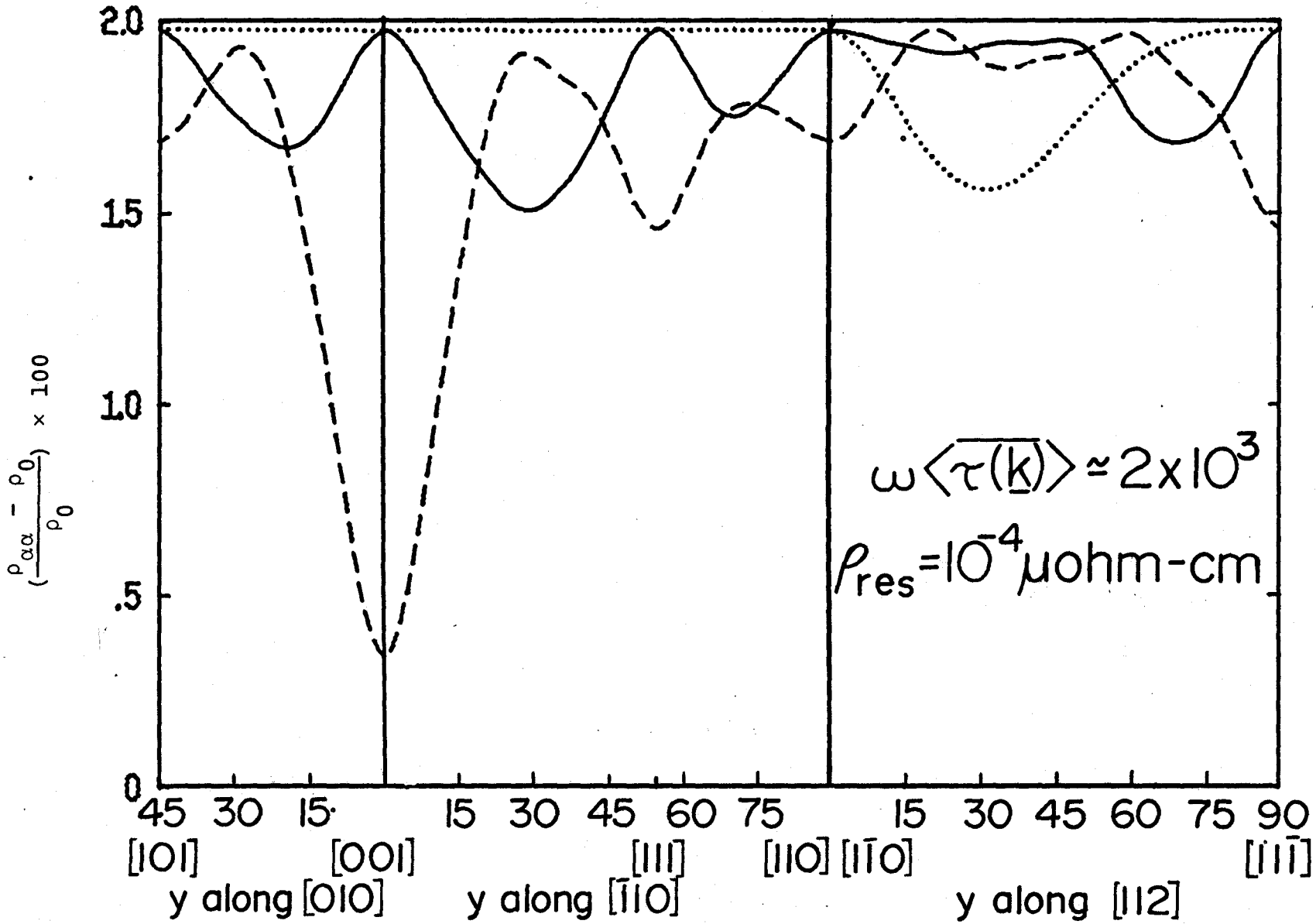
2.0
1.5
1.0
.5
0
$\left(\frac{\rho_{\alpha\alpha} - \rho_0}{\rho_0}\right) \times 100$
$\omega\langle\overline{\tau(\underline{k})}\rangle \simeq 2\times10^3$
$\rho_{res} = 10^{-4}\,\mu$ohm-cm
45 30 15 15 30 45 60 75 15 30 45 60 75 90
[101] [001] [111] [110] [1$\bar{1}$0] [11$\bar{1}$]
y along [010]
y along [$\bar{1}$10]
y along [112]

Fig. 17

Fig. 18: ——— xx • T = 4K , $\rho_{res} = 0$

····· yy

----- zz $\omega\langle\overline{\tau(\underline{k})}\rangle \sim 1$

$\frac{\Delta_{\alpha\alpha}}{\rho_0}$ as a function of orientation.

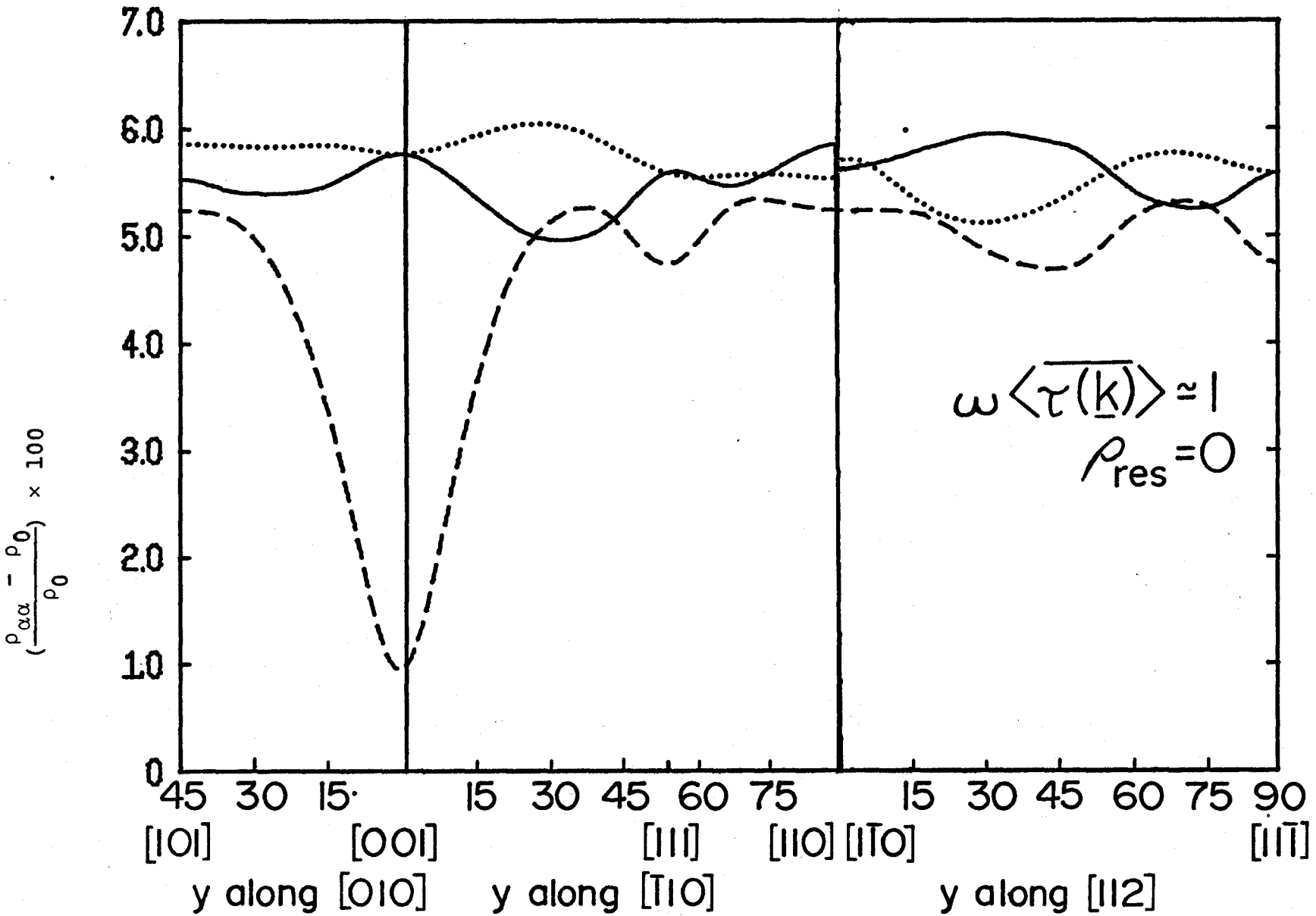
7.0
6.0
5.0
4.0
3.0
2.0
1.0
0
$\left(\frac{\rho_{\alpha\alpha} - \rho_0}{\rho_0}\right) \times 100$
$\omega\langle\overline{\tau(\underline{k})}\rangle \simeq 1$
$\rho_{res} = 0$
45 30 15
15 30 45 60 75
15 30 45 60 75 90
[101] [001] [111] [110] [1$\bar{1}$0] [11$\bar{1}$]
y along [010]
y along [$\bar{1}$10]
y along [112]

Fig. 18

Fig. 19

Small changes in the behaviour of ρ_t were observed, comparable with the experimental uncertainty. However, the behaviour of ρ_l did show significant variation with crystal orientation as is shown in figure 5. Similar variation was found in other samples, including orientations within 5° of [111] and 2° of [110]. It should be noted that the plane normal to [111] contains six [110] type directions, whereas the other field orientations used are such as to pass close to no, or at most two, such directions. The absence of a marked dependence of ρ_t on orientation thus shows that the main influence of crystal anisotropy is found in ρ_l rather than ρ_t.

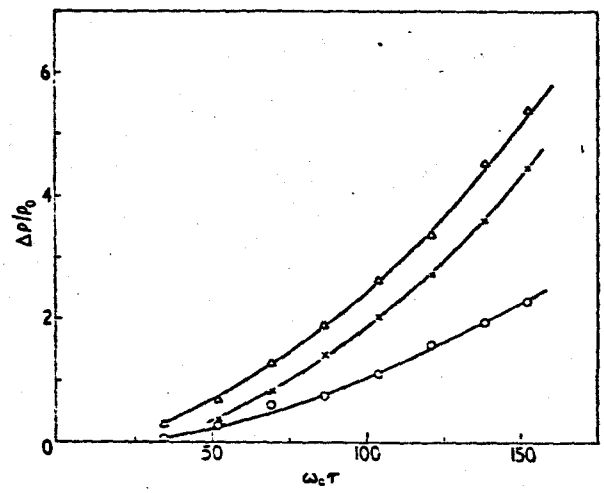

Variation of longitudinal magnetoresistance of K8 with field orientation: O, near [212]: △, tipped 30° toward [$\bar{1}$01]: × tipped 16° more towards [$\bar{1}$01].

Simpson's observations [23] using the soft-helicon method.

soft-helicon method reports variations in Δ_{zz} in the $[1\bar{4}1]$ plane (Fig. 19), while Δ_{xx} and Δ_{yy} are constant to within experimental error. Our calculations show that in this plane, Δ_{zz} has decreased by 2% at 30° away from [212], but drops suddenly to 75% of its initial value around 45° away from [212] (because there $\underline{H}$ passed close to [001]). The discrepancy may have the same causes as the observed 2-fold anisotropy in N_y (see Fig. 19).

In the last two plots (Figs. 20 and 21) percent variations in the induced torque are shown. As expected, the maxima of N_y when $\omega\langle\overline{\tau(\underline{k})}\rangle \sim 1$ correspond to minima when $\omega\langle\overline{\tau(\underline{k})}\rangle >> 1$. The variations are small, but well within the accuracy with which the torque has been measured for aluminum [13]. Unfortunately, measurements of induced torque in potassium have been hard to interpret [15,16], their worst feature being a 2-fold anisotropy which violates crystal symmetry and is large enough to mask the effects predicted here. In the case of the linear magnetoresistance, it seems fairly certain that the effect is not caused by faulty experimental technique, but here the facts are not so well established. (Induced torque measurements [14] confirm the existence of linear magnetoresistance.) The real question which remains to be answered is whether the conditions which cause the linear magnetoresistance and anomalous torques are ever absent in nature. If not, Eq. (I.30) is meaningless because some essential feature of potassium was not built into the model that generated it.

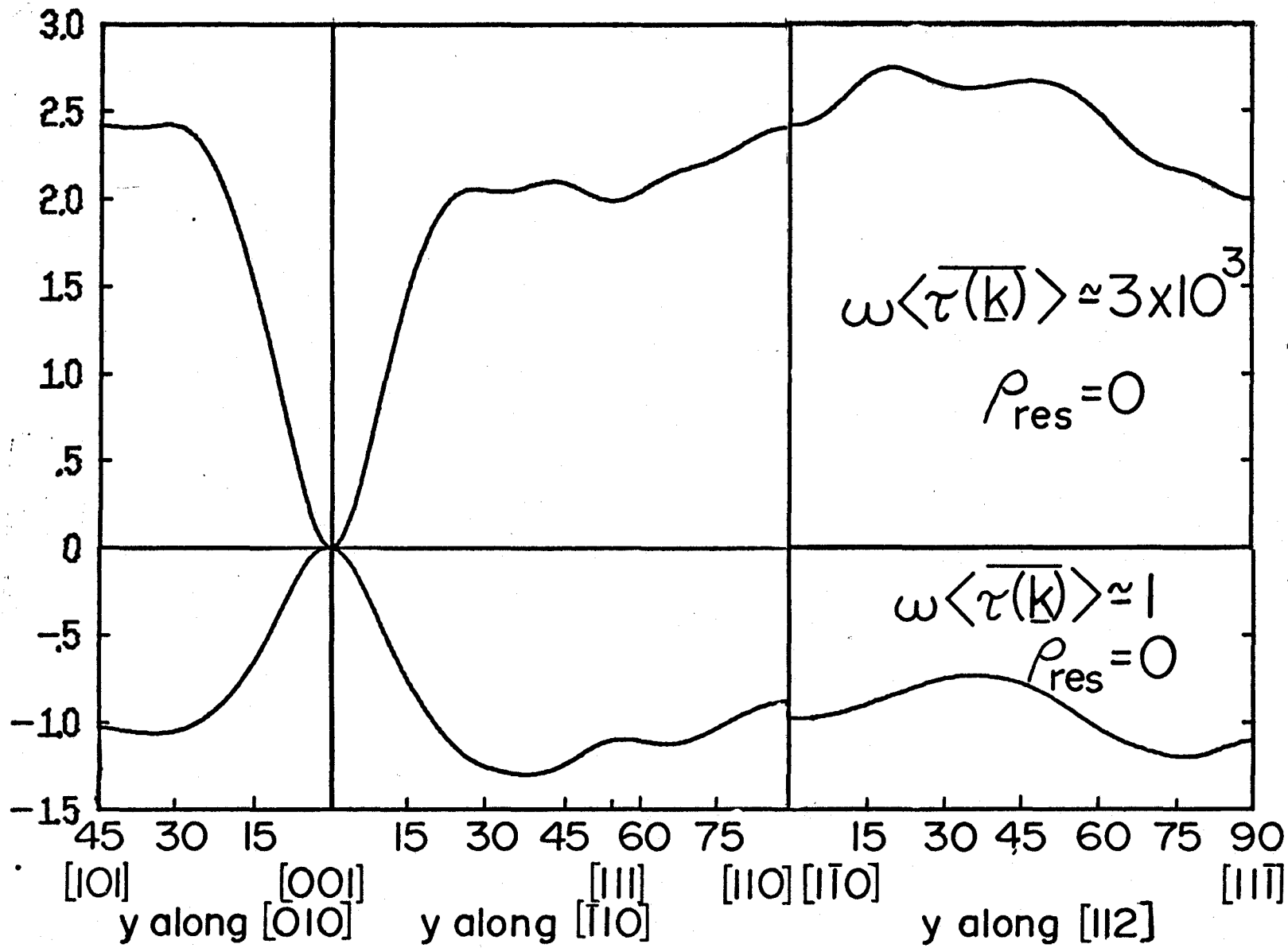

Fig. 20

Anisotropy in the induced torque at high and intermediate fields. T = 4K.

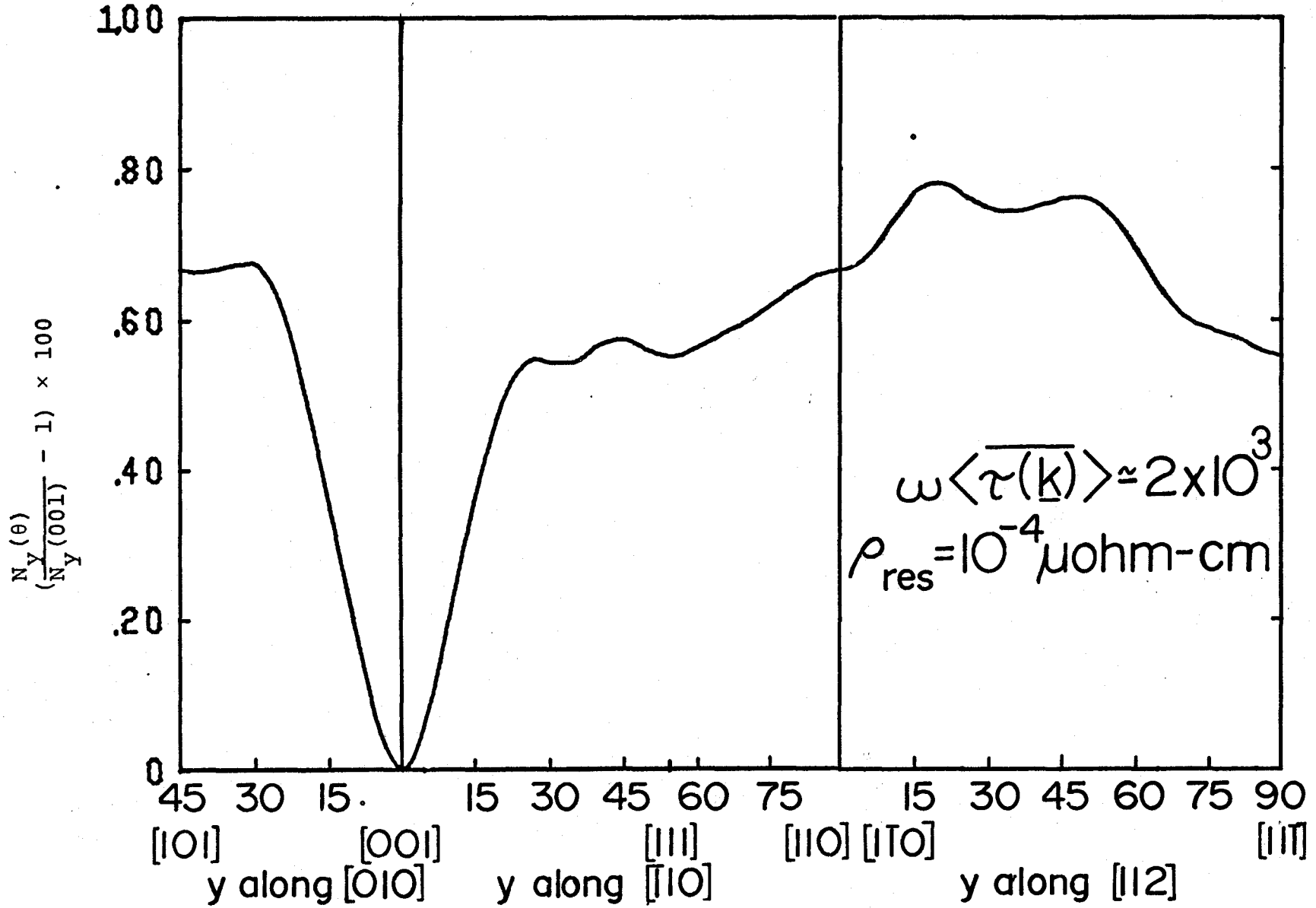

Fig. 21

Anisotropy in the induced torque in an impure sample at 4K.

CHAPTER IV

CONCLUSION

Numerical integration of a simple semi-classical expression for the conductivity tensor in a magnetic field for a one-electron metal with a spherical F.S. suggests that under optimum conditions (pure metal at the temperature when the scattering time $\tau(\underline{k})$ anisotropy is maximum) a magnetoresistance of about 7% or slightly greater should be seen. This magnetoresistance reaches a saturation value which depends on the orientation of the magnetic field with respect to the crystal axes. The longitudinal magnetoresistance is most sensitive to orientation and the functional form of $\tau(\underline{k})$; the transverse magnetoresistance displays smaller variations related more to crystal symmetry. Such variations in the magnetoresistance are sufficient to cause a maximum 2% anisotropy dictated by crystal symmetry and by the form of $\tau(\underline{k})$ in the induced torque.

The preceding summary of theoretical and computational results does not tie in very well with experimental results. The saturation of the magnetoresistance predicted by our theory is not observed. This is a disturbing fact and probably indicates the model behind the theory is an oversimplification. Nevertheless some features at least of

the magnetoresistance (its temperature dependence) are qualitatively in accord with our computations, so the model cannot be completely out of touch with reality.

REFERENCES

1. H. Jones and C. Zener 1934 Proc. Roy. Soc. A144 101.
2. F. Seitz 1950 Phys. Rev. 79 372.
3. J. M. Ziman 1961 Adv. Phys. 10 1.
4. W. Shockley 1950 Phys. Rev. 79 191.
5. R. G. Chambers 1956 Proc. Roy. Soc. A238 344.
6. G. Wannier 1972 Phys. Rev. B 5 3836.
7. V. G. Visscher and L. M. Falicov 1970 Phys. Rev. B 2 1518.
8. B. Hayman and J. P. Carbotte 1972 J. Phys. F 2 915.
9. R. J. Douglas and W. R. Datars 1973 Can. J. Phys. 51 1770.
10. J. Babiskin and P. G. Siebenmann 1971 Phys. Rev. Lett. 27 1361.
11. B. Hayman and J. P. Carbotte 1972 Phys. Rev. B 6 1154.
12. J. W. Ekin and B. W. Maxfield 1971 Phys. Rev. B 4 4215.
13. F. W. Holroyd, R. J. Douglas and W. R. Datars 1973 Can. J. Phys. 51 1786.
14. J. S. Lars and A. B. Pippard 1970 J. Phys. E 3 137.
15. J. A. Schaeffer and J. A. Marcus 1971 Phys. Rev. Lett. 27 14.

16. T. K. Hunt and S. A. Warner 1973 Proceedings of LT13 IV 78.

17. D. Shoenberg and P. J. Stiles 1964 Proc. Roy. Soc. A281 62.

18. K. Okumura and I. M. Templeton 1965 Proc. Roy. Soc. A287 89.

19. R. C. Leavens and J. P. Carbotte 1973 Can. J. Phys. 51 398.

20. A. W. Overhauser 1971 Phys. Rev. B 3 3173.

21. E. Justi and K. Auch 1964 Z. Naturforsch. 18 767.

22. R. A. Young 1968 Phys. Rev. 175 813.

23. J. Simpson 1973 J. Phys. F 3 1471.

24. B. Hayman and J. P. Carbotte 1972 Phys. Rev. B 6 4.

25. B. White, Z. Popović and J. P. Carbotte to be published.